2015

Crack separation mechanism applied in CO2 laser machining of thick Polycrystalline Cubic Nitride (PCBN) tool blanks

Yixian Wang
Iowa State University

Crack separation mechanism applied in CO2 laser machining of thick Polycrystalline Cubic Nitride (PCBN) tool blanks

by

Yixian Wang

A thesis submitted to the graduate faculty

in partial fulfillment of the requirements for the degree of

MASTER OF SCIENCE

Major: Mechanical Engineering

Program of Study Committee:
Pranav Shrotriya, Major Professor
Ganesh Balasubramanian
Robert W. Stephenson

Iowa State University

Ames, Iowa

2015

TABLE OF CONTENTS

ACKNOWLEDGEMENTS

I sincerely appreciate my major professor, Dr. Pranav Shrotriya. His precious guidance, suggestions as well as motivation always supported me whenever I encountered a dilemma. I honestly cherish the precious and wonderful time working with him.

I would like to express my gratitude to my former major professor, Dr. Pal A. Molian, who gave the platform and opportunity to work in the research area. His patient mentoring and assiduous attitude always inspire and help me a lot. Another two committee members I would like to thank are Dr. Robert W. Stephenson, and Dr. Ganesh Balasubramanian, for having spent time being my committee and professional guide. I also want to mention my co-workers/lab-mates for their timely and technical support especially for Ammar A. Melaibari, a real researcher has published tens of papers and provided me support; Zhuoru Wu, who helped me with the modeling work. I also would like to acknowledge Tugce Karakulak, Xiaoduan Tang and Can Zhu, who coached and helped me with scanning electron microscopy and Raman spectroscopy.

I would like to acknowledge the support by the National Science Foundation under the grant CMMI-100035. Whilst, I want to gratefully appreciate the donation of BZN 7000S samples by Diamond Innovations, INC, Worthington, OH.

At last, I would like to forward my sincere gratitude to my parents, grandmother and friends. It is your encouragement, support as well as love that offer me the courage and confidence to face to any challenges and trouble. Were it not for you this work could not accomplish.

ABSTRACT

The main objectives of this work are: (1) to explore and improve the hybrid CO_2 laser/waterjet (LWJ) technique, developed by Iowa State University's Laboratory for Lasers, MEMS and Nanotechnology, to machine thick polycrystalline cubic boron nitride (PCBN) tool blanks both in 1D and 2D with minimum energy consumption and good cut quality; (2) to examine the mechanism of crack separation in the cutting process, both experimentally and numerically to increase the consistency of laser performance and manufacturing feasibility. The LWJ process showed advantages over conventional methods such as wire-EDM and pulsed Nd:YAG laser. The wire-EDM is not applicable for electrically insulating solid form PCBN tools and the pulsed Nd:YAG laser suffers from poor cut quality and low cutting speed. In this work, a 4.8-mm-thick specimen in solid form was cut successfully, both in 1D and 2D using nitrogen as an assist gas. The cut quality and governing mechanism were studied by electrical microscopy (SEM/EDS), Raman spectroscopy and optical profilometer. Statistical design of experiment was applied to help design and optimize the consistency of the cutting experiment. Numerical model based upon finite element analysis was also used to validate the mechanism and predict the surface profiles and fracture behavior. There are good agreement between experimental measurements and modeling results.

CHAPTER 1

INTRODUCTION

1.1 Background of Polycrystalline Cubic Boron Nitride (PCBN) tools

Cubic boron nitride (cBN) is a super-hard material. It is harder than all other material except diamond. However, it is harder than diamond when temperature rises above 700 ˚C. Other intriguing properties include exceptional thermal and chemical stability as well as superior mechanical properties, such as high Young's modulus, high thermal conductivity (50-200 W/mK), extreme high wear resistance, and a low friction coefficient. cBN powders are synthesized with metallic binders (Co) or ceramic binders (AlN or TiN) under extremely high temperature and pressure conditions to form homogenous polycrystalline cubic boron nitride (PCBN) tool blanks [1]. It retains constant hardness in elevated temperature and inertness to iron. A PCBN tool is an ideal cutting tool for machining hardened ferrous material and takes the place of conventional grinding processes, especially for high speed cutting, milling or turning and finish machining on hard cast iron, high chrome alloy steel, high-strength nickel super-alloys and powder metal alloys [2].

PCBN tools are machined in two forms: a composite bonded to a cemented substrate or self- supported. Such tool blanks are usually machined into dies and index inserts. PCBN index inserts ranging from 1.6mm to 4.8mm in thickness are available in round, triangle, square and rhombus (55°, 80°, 35°) geometries with chamfered or unchamfered edges in order to fit standard negative rake angle tool holders.

1.2 State-of -the-art manufacturing methods for PCBN inserts

PCBN tool inserts exhibit outstanding cutting performance with exceptional tool life; however, it is formidable to machine different shapes of dies or inserts due to its superhigh hardness and brittleness. In terms of tool production, speed, resolution and cost-effectiveness are the most important criteria required. Diamond sawing, electric discharge machining (EDM), electrical discharge grinding (EDG) and conventional Nd:YAG laser cutting are among the most popular techniques.

Diamond sawing is rarely utilized in the current market due to its low efficiency, rapid tool wear and poor precision. Also, it is limited to straight cuts and large kerfs owing to the thickness of the blade. Wire-EDM and EDG are restricted to electrical conductive materials, and so are not feasible for those PCBN tools without Co or TiN binders. High energy consumption and slowness have limited its further development and application. Conventional pulsed Nd:YAG laser overcome some deficiencies of EDM/EDG processes; for instance, a Nd:YAG laser could cut ultra-hard materials like polycrystalline diamond (PCD) and PCBN at a speed of 80-100 inch per minute[3]. However, it still suffers from low tolerance and velocity due to laser ablation mechanism such as multiple passes with fine feed each time required to cut through the whole thickness of tool blanks. In addition, particle formation, thermal damage and conical kerfs generation call for post treatment like polishing and brazing to meet finish requirements.

Given the drawbacks of the conventional laser, Synova S. A. Switzerland pioneered and patented an extension of pulsed Nd:YAG laser cutting called Laser-Microjet® (LMJ®), where a waterjet is added to deliver the 532 nm Nd:YAG beam [4]. The high-pressure waterjet aids in reducing the spot size and thermal damage in the laser-cut zone while not changing the material removal mechanism. The LMJ for cutting 4.8 mm thick PCBN yielded improved cut quality with

little change in cutting speed. Approximately 70 to 90 laser passes were required at an overall speed of 6-6.85 mm/min [5].

1.3 Improved CO2 Laser/Waterjet (CO2-LWJ) mechanism and method

Though LMJ® procedures good surface finish with negligible thermal damage, no burrs and post-processing free, the mechanism still remains as laser ablation, resulting in slow speed and calling for novel improvement. Lumely [6] first applied a controlled fracture mechanism in machining brittle material such as glasses by utilizing a single CO_2 laser to scribe a substrate and propagate a fracture controllably. The laser power used was lower than past methods and cutting speed was also much faster. Tsai and Chen [7] extended the method to cutting aluminum oxide with one focused beam aimed at groove forming, another defocused beam to initiate the crack and propagate the crack through the thickness. Specimens of 10 mm thickness were cut through successfully both in a straight line and a curve.

A non-traditional hybrid CO_2 laser/waterjet process was developed by a group of researchers at Iowa State University to investigate the feasibility of applying a crack separation mechanism in machining superhard material such as polycrystalline diamond (PVD) and PCBN, that meets the manufacturing specifications and could become an alternative to current methods. Unlike conventional energy-intensive erosive wear or melting blow and subsequent evaporation, the group combined a 10.6 μm continuous wave CO_2 laser with low-pressure abrasive free waterjet synergistically such that the material removed by thermal shock assisted fracturing the material into fine fragments. Fig. 1 shows the schematic of CO_2-LWJ process. The workpiece first undergoes laser irradiating, groove forming, and water quenching and then causes crack propagation with material separation. Two main driving forces guide the whole process

according to our previous study: one is the thermal stress induced by rapid water cooling right after the laser is heated, another is the mechanical stress caused by phase transformation especially sp^3 to sp^2 (e.g. diamond to graphite phase), which will increase brittleness of the machined region and volumetric expansion which in turn facilitates the controlled fracture propagation.

It has been successfully demonstrated that the ability of the LWJ process to machine PCD and cubic boron nitride (cBN) dies in one dimension. The relationship between machining parameters and fracture characteristics has been studied both experimentally and numerically. A two-dimensional contour cut performed well in thin PCBN both in a WC-supported form and a solid form. Different fluid media effects were also explored to identify the best candidate for machining PCBN material. Nitrogen provided high transition depth, less energy consumption and less thermal damage. The LWJ process made controllable crack separation, a smooth machined surface and negligible thermal defects. Given the benefits of two media, an improved extension of nitrogen-assisted the LWJ process was explored especially during two-dimensional cutting of thick PCBN.

1.4 Thesis organization

This thesis consists of four chapters: Chapter 1 is a brief introduction for the foundation process of LWJ technique and PCBN tools. Chapters 2 and 3 are in journal paper format. Chapter 2 focuses on identifying the effects of N_2 and a water assisted process in one-dimensional cutting. Statistical design of experiments is applied in experiment development and optimization. Chapter 3 explores a new method called N_2-assisted LWJ during two-dimensional cutting. Numerical FEM analytical results are included to compare with the experimental

measurements. Chapter 4 presents the fundamental conclusions based upon the current research and tasks in the future.

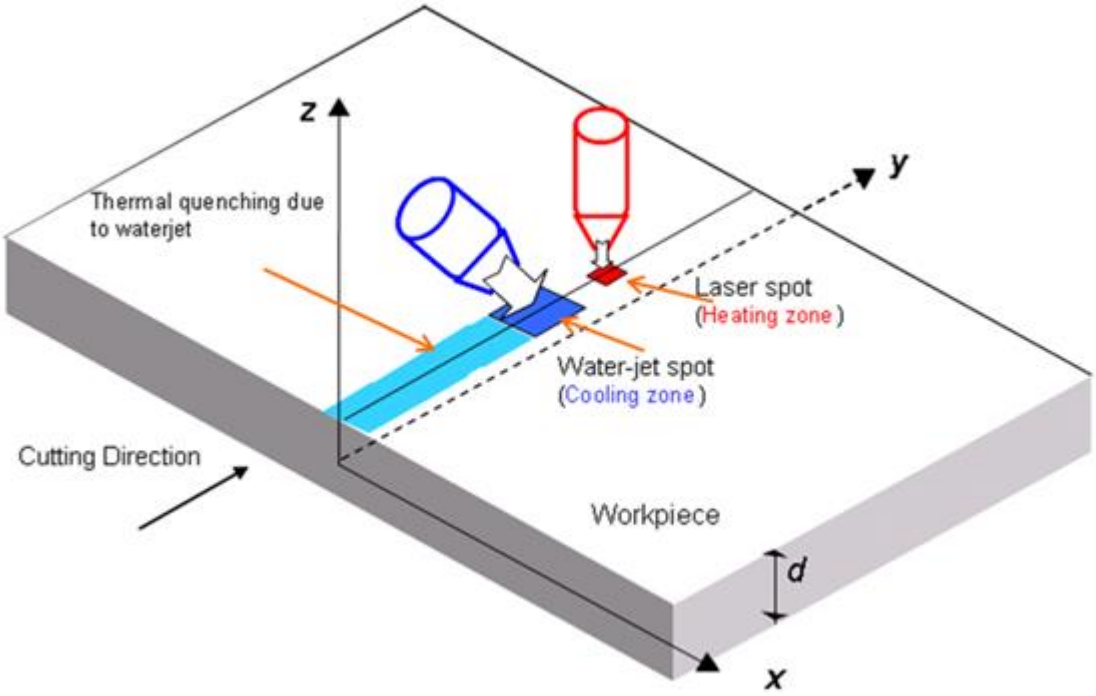

Fig.1 The schematic of CO_2-LWJ process

1.5 References

[1] Wentorf RH (1957) Cubic form of boron nitride. J Chem Phys 26(4):956.

[2] Ding X, Liew WYH, Liu XD (2005) Evaluation of machining performance of MMC with PCBN and PCD tools. Wear 259(7-12):1225-1234.

[3] http://www.qs-diamondtechnology.com/Pages/LDMachines.aspx Accessed on 21 April 2013.

[4] http://www.swissphotonics.net/libraries.files/SwissLaserNet_11.09.pdf. Accessed on 21 April 2013.

[5] Pauchard A, Marco MD, Carron B et al (2008) Recent developments in the cutting of ultra hard materials using water jet-guided laser technology, ALAC conference, Minneapolis.

[6] Lumely, R. M., 1969, Am. Ceram. Soc. Bull., 48(pp. 850-854.

[7] Tsai, C.-H., and Chen, H.-W., 2003, "Laser Cutting of Thick Ceramic Substrates by Controlled Fracture Technique," Journal of Materials Processing Technology, 136(1-3), pp. 166-173.

CHAPTER 2

CRACK SEPARATION MECHANISM IN CO_2 LASER MACHINING OF THICK POLYCRYSTALLINE CUBIC BORON NITRIDE TOOL BLANKS

A paper published in the International Journal of Advanced Manufacturing Technology, Feb, 2014

Yixian Wang, Pal Molian and Pranav Shrotriya

Abstract

An improved method for cutting thick polycrystalline cubic boron nitride (PCBN) tool blanks is explored because current methods of pulsed Nd:YAG laser cutting and wire electric discharge machining (EDM) are constrained by low speed and low precision. We present a CO_2 laser/waterjet (LWJ) process to cut 4.8 mm thick PCBN tool inserts by a crack separation mechanism. In LWJ, the PCBN blank is locally heated using a high-power continuous wave CO_2 laser to cause phase transition from cubic to hexagonal followed by water quenching to generate thermal stresses and form boron oxide leading to increased brittleness, subsequent cracking, and material separation. A 2^3 factorial design of experiment (DOE) approach was employed to determine the factors of laser power, cutting speed and waterjet pressure on the responses of phase transformation depth, taper, and R_a. A numerical heat flow model, based on Green's function, was used to calculate the temperature distributions along the depth. Surface profilometer, scanning electron microscopy and Raman spectroscopy were utilized to analyze the phase transformation and crack zones. Results from LWJ compared with pulsed Nd:YAG laser and laser microjet™ methods indicate LWJ cuts 30 times faster; this was attributed to a non-

conventional material removal (crack separation) mechanism. When LWJ was compared against nitrogen-assisted CO_2 laser cutting, improved cut quality (less taper and smaller heat affected zone) was observed due to a greater control on phase transformation and crack propagation. DOE analysis revealed laser power and waterjet pressure and the interactions among them are more significant factors than others.

Keywords: Cubic boron nitride; CO_2 laser; Waterjet; Crack separation mechanism; Design of experiment

2.1 Introduction

Polycrystalline cubic boron nitride (PCBN) ranks as the second hardest (30-45 GPa) tool material on earth. It is a synthetic material composed of cubic boron nitride (cBN) particles in a ceramic matrix, like TiN or AlN, and produced under extreme pressure and temperature conditions [1]. It is an ideal tool material for efficient, precision machining of hardened ferrous and non-ferrous alloys, such as pearlitic grey cast irons, nickel and cobalt-based alloys, hardened steels, powder metal irons, hard facing alloys and superalloys [2] by virtue of excellent hardness, wear resistance and thermal stability. There are two basic tool forms for PCBN: (1) brazed on tungsten carbide, and (2) solid form. The latter is advantageous because it can be used as a double edged tool. A solid PCBN insert is also the best choice for rough machining of cast irons and steels.

PCBN tool inserts in the solid form are traditionally produced by a sequence of processes (Fig.1) that involve powder metallurgy sintering of cBN powders with a binder to form a disc; cutting of the disc by wire electrical discharge machining (EDM) or pulsed Nd:YAG laser to

form inserts; and then finishing the inserts to obtain the desired surface finish and tolerance. Tool inserts can be made in different geometries, such as squares, diamonds and triangles.

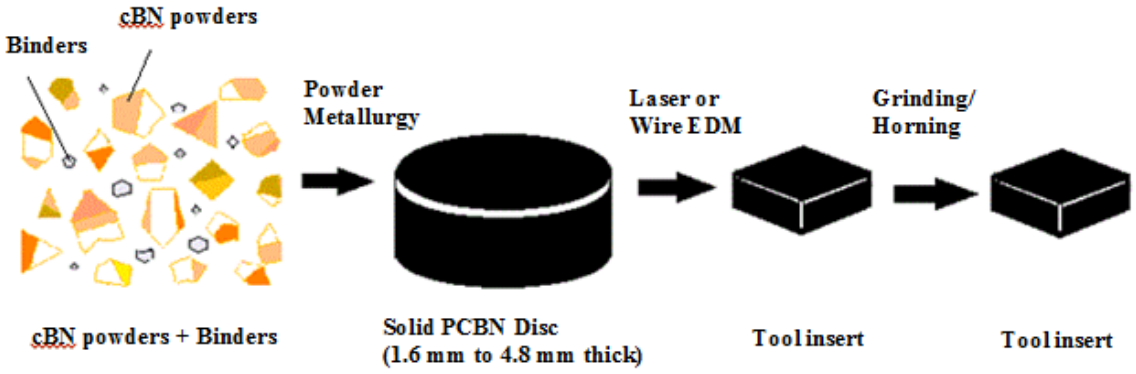

Fig. 1 Schematic diagram showing process flow for PCBN tool inserts

Wire EDM is a slow process and is further limited by the electrical conductivity of PCBN. Essentially the electrical conductivity of the binder material used for sintering PCBN discs dictates the ability of EDM to cut PCBN. On the other hand, EDM can reduce tooling cost and allow for more precise geometries generation. Pulsed Nd:YAG laser is advantageous over wire EDM in faster cutting (about 30 times). Yet pulsed Nd:YAG laser cutting of PCBN up to 6 mm thick is accomplished at slow speeds (<10 mm/min) with low precision due to recast layer formation, taper, thermal damage, and rough surface [3].

Pulsed Nd:YAG laser cutting of PCBN tool blanks involves evaporation and sublimation as the material removal mechanisms. Pulse widths from nanoseconds to microseconds with an average power of 40 to 120 W in the speed range of 5 to 10 mm/min are generally used for a kerf width of about 0.1 mm [4]. Ablation rate in micrometers per pulse occurs; thus, hundreds of multiple passes are needed to cut through the entire thickness of the sample. The process often results in thermal damage and recast layer formation. Figure 2 shows the morphology of a laser-cut surface of 4.8 mm thick PCBN, showing non-uniform ablation on the microscale and the presence of microcracks in cBN particles. Figure 3 shows the surface roughness profile recorded

by the optical profilometer. The average surface roughness is Ra 3 μm. Further analysis revealed that no phase transformation such as cBN→ hBN has occurred during cutting.

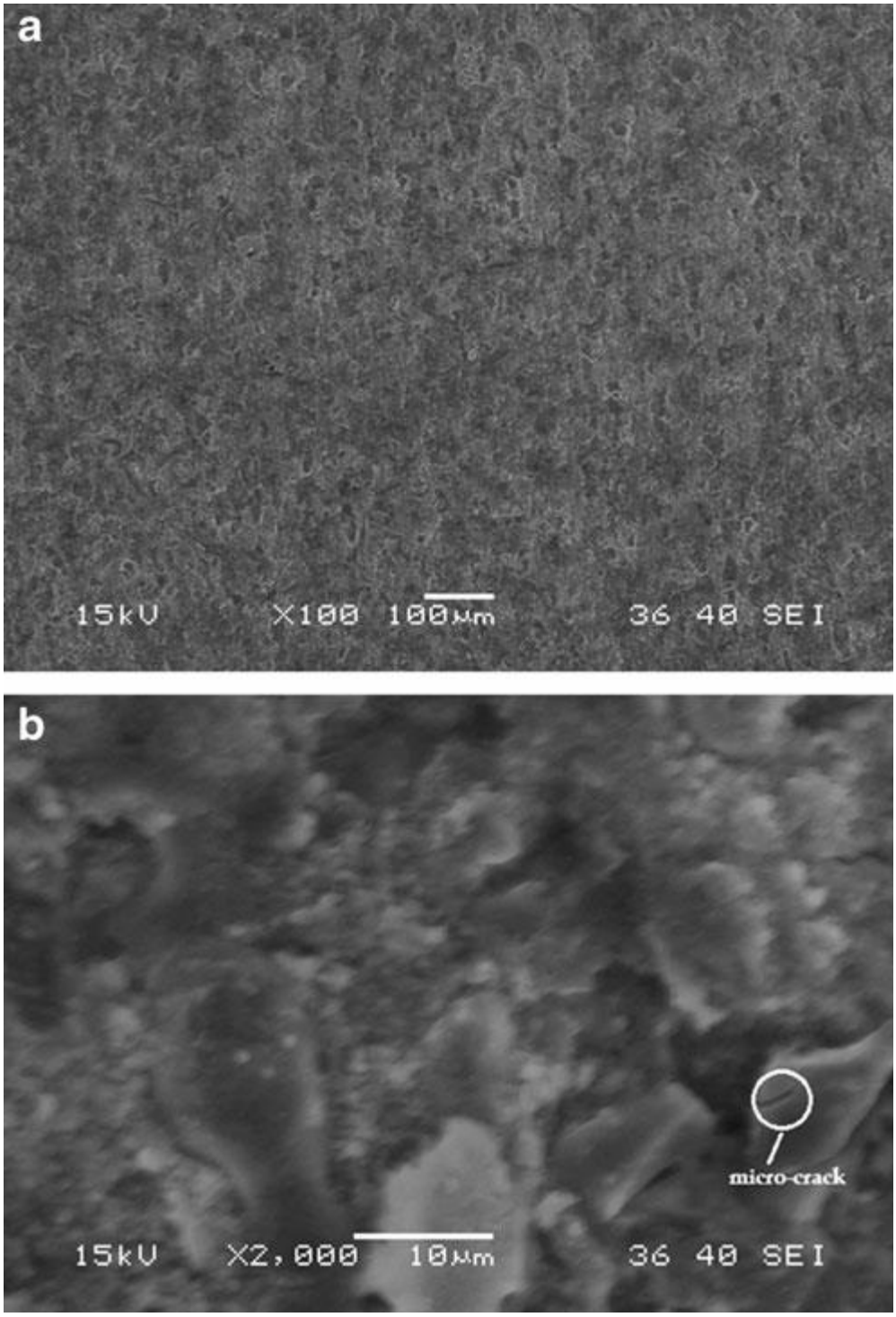

Fig. 2 SEM images of the cross-section of PCBN cut by conventional laser: (a) low magnification micrograph showing the pattern of non-uniform ablation; (b) high magnification micrograph showing the presence of microcrack in cBN particles.

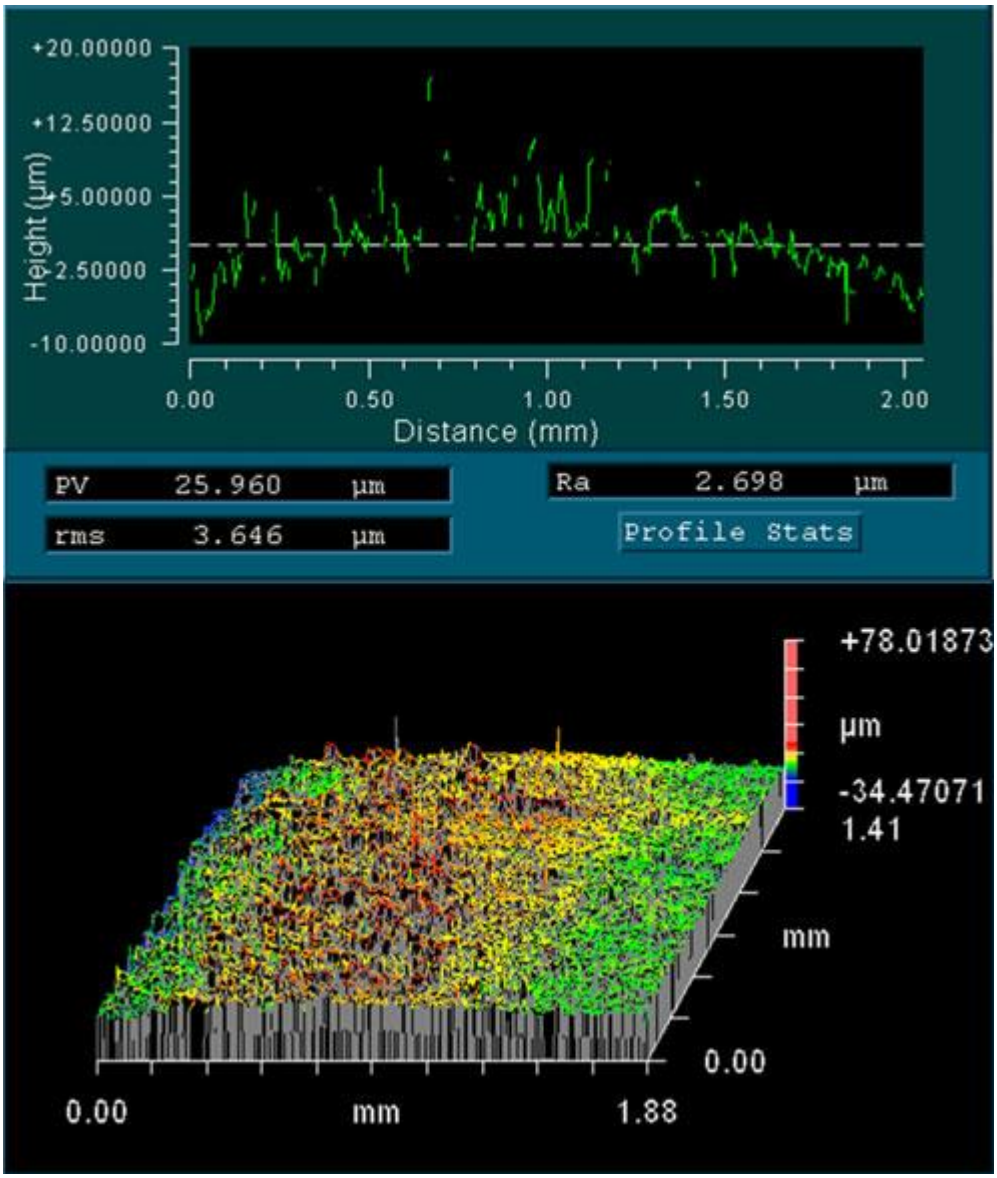

Fig. 3 3D topography and surface profile of conventional laser-cut PCBN

An extension of traditional pulsed Nd:YAG laser cutting is Laser-Microjet® (LMJ®), where a waterjet is added to deliver the 532 nm Nd:YAG beam [5]. The waterjet aids in reducing the spot size and thermal damage of laser-cut zone while not changing the material removal mechanism. The LMJ® for cutting 4.8 mm thick PCBN yielded improved cut quality with little change in cutting speed. Approximately 70 to 90 laser passes were required at an overall speed of 6 mm/min [6].

Producing a precise and high-quality PCBN tool insert at high speeds still remains as a formidable challenge. The desirable characteristics of tool inserts include small cutting width, parallel kerf, minimal heat affected zone, smooth surface, and little taper. To meet these requirements, a low energy cutting process must be employed. In this work, we have applied a continuous wave CO_2 laser for cutting 4.8 mm thick PCBN samples in two different ways: (1) use of nitrogen assist gas and (2) combine the laser beam with a waterjet (LWJ). Previously we have applied such techniques to cut 1.6 mm thick PCBN samples in the solid form [7-9] and discovered some improvements in cutting speed and cut quality. However, this work was not comprehensive to establish the effects of laser parameters and to understand the various aspects such as phase transformation depth, taper and surface roughness. Previous work was also limited to thin sections. Hence, in this work, we made a detailed study of cutting 4.8 mm thick PCBN tool blanks and associated material removal mechanisms. In addition, a 2^3 factorial design methodology was applied to evaluate the effects of laser power, cutting speed, and nitrogen gas pressure or waterjet pressure on responses such as surface roughness, transformation depth and taper angle. Both main effects and interaction effects were determined. Such a DOE approach will facilitate eliminating numerous trial-and-error scenarios currently required to select and tune these parameters for industrial applications.

2.2 Experimental details

2.2.1 Material

PCBN tool blanks (BZN 7000S, electrically nonconductive) composed of 82% cBN and 18% AlN were procured from Diamond Innovations, Inc. (Ohio) in 4.8 mm thick solid form. Surface roughness (Ra) for the polished blanks was measured by optical profilometer as 0.3 µm. Figure 4 shows the microstructure of BZN 7000S that exhibits a grain size of 15 µm. The pulsed Nd:YAG laser is currently used to cut BZN 7000S blanks because wire EDM is not suitable. The thermal properties for BZN 7000S, estimated based on volume fractions cBN and AlN, are listed in Table 1.

Table 1 Estimated thermal properties of BZN 7000S

Thermal conductivity (W/mK)	**Specific heat capacity (J/kgK)**	**Density (kg/m^3)**	**Thermal diffusivity (m/s^2)**
189	871	3412	6.36×10^{-5}

2.2.2 Methods

A continuous wave CO_2 laser (Model 820 Spectra Physics) of 10.6 µm wavelength and 1500 W rated power was utilized in all experiments. The laser power varied from 400 to 800 W, while the cutting speed was increased from 4 to 13 mm/sec. The beam was focused to a spot size of 0.2 mm, using a 127 mm focal length lens. Two experiments were conducted. The first experiment consisted of laser cutting the PCBN samples with nitrogen as the assist gas. Nitrogen was chosen over oxygen or air to prevent oxide formation, uncontrolled fracture, and lower

groove depth. Nitrogen also facilitates material removal by momentum effects and minimizes heat damage by cooling effects. The beam and gas were transmitted coaxially through a 1 mm diameter copper nozzle. The sample was mounted on an X-Y positioning table guided by a computer numerical controller (CNC). The standoff distance between the specimen surface and the nozzle was set at about 1 mm. The second experiment was achieved with the aid of a waterjet (LWJ). The details of LWJ are described elsewhere [7-9]. The beam was focused to a spot size of 0.2 mm as in the previous case. A special cutting head with two holes (Fig.5), the central hole for the laser beam and the other hole for the waterjet, was used. The diameter of the waterjet was 0.33 mm. The distance between the two holes was 2 mm to eliminate the beam directly interacting with the water. It may be noted that water absorbs nearly 70% laser energy at CO_2 laser wavelength. Air was used coaxially with the laser beam to further prevent beam interaction with water and also splashing of water onto the lens.

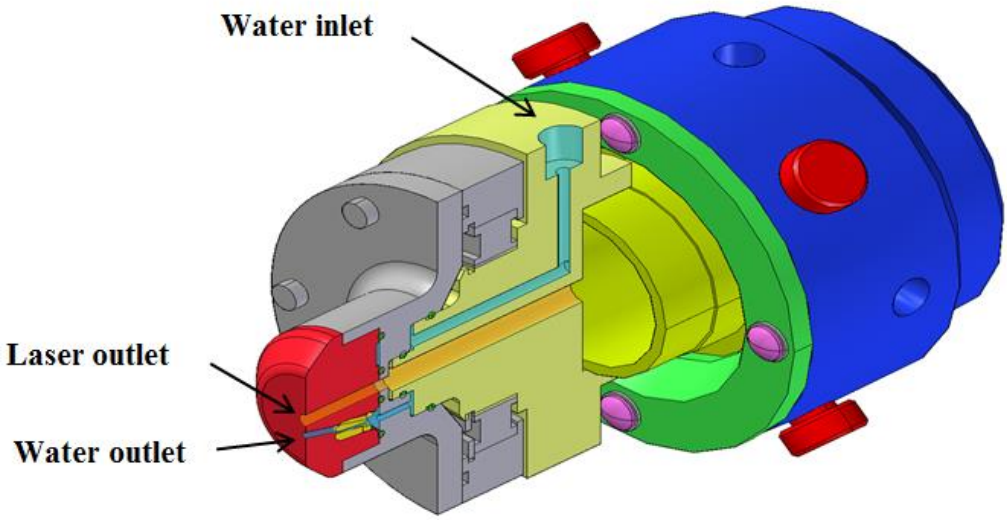

Fig. 5 Laser/waterjet cutting head

2.2.3 Design of experiments

Although not an optimization tool, the factorial design of experiment offers identification of the main and interaction effects of the input variables on responses with a minimum number of experiments. The purpose of DOE in this work was to identify the significance of the factors that affect cut quality. Three factors of interest were investigated in this study: (1) laser power, (2) cutting speed and (3) nitrogen gas or waterjet pressure. A 2^3 factorial design was set up with two levels for each factor, listed in Tables 2 and 3. The remaining factors, such as beam diameter, focal length of lens, beam mode, standoff distance, and focus position were kept constant. The response of cut quality is expressed in terms of R_a, taper and phase transformation depth. To keep the number of experiments and subsequent analysis manageable, two replications for each experiment were performed. R_a was quantified with the help of a profilometer and converted into a rating scale of 1 to 5 (Table 4). Taper was also measured and converted into a rating scale (Table 4).

Table 2 Factors and their levels of nitrogen-assisted CO_2 laser cutting experiment

Factors of interest	Low level (-)	High level (+)
Laser power (W)	400	800
Cutting speed (mm/sec)	4	13
Gas pressure (kPa)	68.9	137.9

Table 3 Factors and their levels of waterjet-assisted CO_2 laser cutting experiment

Factors of interest	Low level (-)	High level (+)
Laser power (W)	400	800
Cutting speed (mm/sec)	4	13
Waterjet pressure (kPa)	413.7	6895

Table 4 Scale for R_a and taper ratings

Scale	Surface Roughness	Taper
1	Surface roughness in Ra < 1 μm	Zero degree
2	Surface roughness in Ra 1-3 μm	1 to 5 degrees
3	Surface roughness in Ra 4-7 μm	5 to 10 degrees
4	Surface roughness in Ra 7-10 μm	10 to 15 degrees
5	Surface roughness in Ra > 10 μm	>15 degrees

2.2.4 Analysis

An optical profilometer (Zygo NewView 7100) with 5× and 20× magnifications was utilized to measure and analyze the kerf profile, groove depth and surface roughness. Groove depth was basically the phase transformation depth. An optical microscope was used to accurately measure the transformation depth in through-cut samples with a resolution of 1 μm. Scanning electron microscopy (SEM Model JOEL JSM-606LV at 20kV) was used to examine the phase transformation and crack propagation zones. Raman spectroscopy (532 nm using Ar-ion laser) was utilized to identify the phase signatures.

2.3 Results and discussion

2.3.1 Nitrogen-assisted CO2 laser cutting

Figure 6 is a plot of line energy against type of cutting categorized, such as scribing, cutting, and uncontrolled fracture. Line energy in laser cutting is defined as P/V^m, where P = laser power, V = cutting speed, and $m \leq 1$. Experiments with two different powers and cutting

speeds indicated m=0.63 for our case. Threshold line energies required for cut-through and uncontrolled fracture were approximately 12,000 and 14,000 J/m, respectively. Higher gas pressure causes uncontrolled fracture at higher line energy due to additional stress effects. The kerf width in all cases was about 0.2 mm (same as spot size). Figures 7 and 8 show the secondary electron images of the cross sections of through-cuts in PCBN at 400 and 800 W, respectively. Two zones may be noted: (1) phase transformation zone with a depth the same as the groove depth produced by thermal evaporation or decomposition of PCBN and (2) fracture zone caused by crack separation. It may be noted the boundary between these two zones is non-uniform. Furthermore the fracture zone had a surface roughness of Ra 4 μm, as measured by the mechanical probe profilometer. It was difficult to use the optical profilometer, due to considerable waviness in the fracture zone.

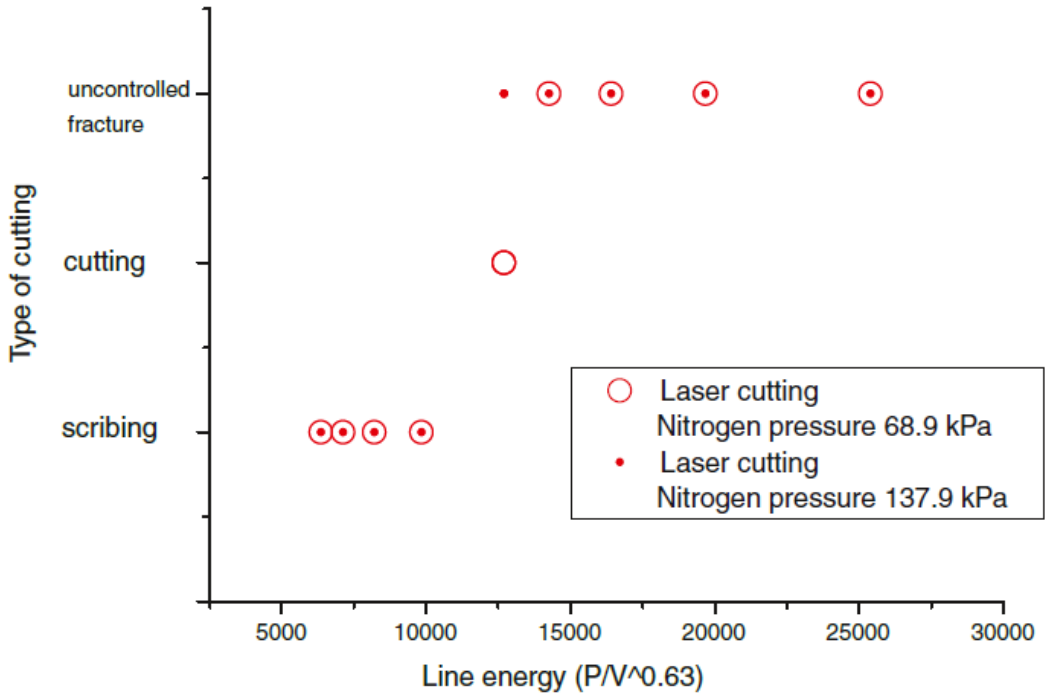

Fig. 6 Effect of line energy on the type of cutting mechanism in nitrogen-assisted laser cutting

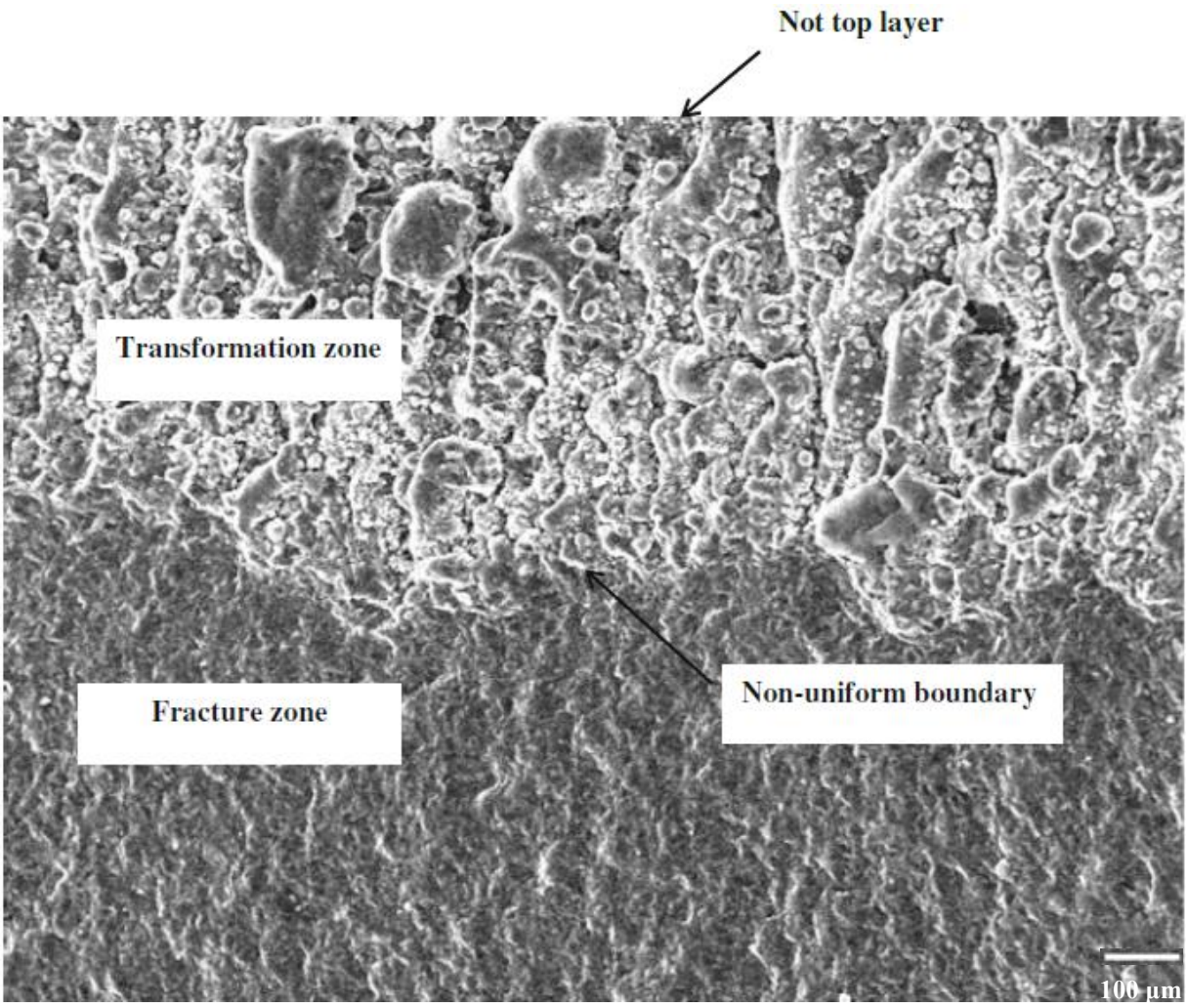

Fig. 7 SEM images of 137.9 kPa nitrogen-assisted laser machined cross section at 400W, 4mm/s (×100)

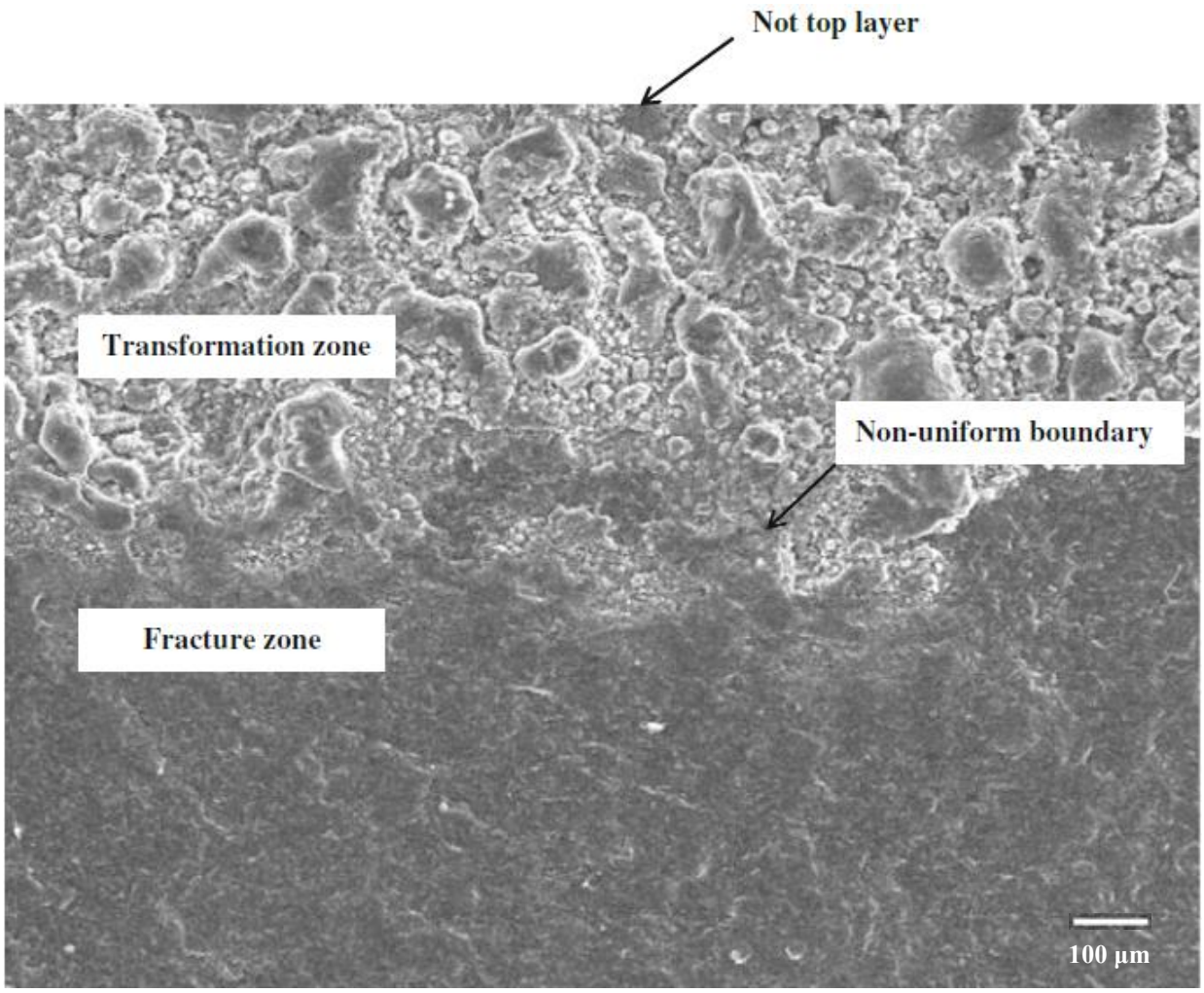

Fig. 8 SEM images of 137.9 kPa nitrogen-assisted laser machined cross section at 800W, 13mm/s (×100)

Figure 9 shows the Raman spectra of phase transformation and fracture regions. Before we analyze the Raman data, the phases corresponding to different peaks must be recognized. Table 5 lists the positions of Raman peaks for various allotropes of BN. The fracture zone is similar to as-received material with peaks characteristic of cBN phase. However, the phase transformation zone is composed of cBN (1055 cm^{-1}), hBN (1365 cm^{-1}) and eBN (1555 cm^{-1}), suggesting a phase transition from cBN to hBN and eBN. Explosive BN (eBN) is a metastable,

octahedral phase with a typical particle size of 30 to 120 nm, formed during the transformation between cBN and hBN under high pressures and high temperatures [10]. It was reported cBN undergoes phase transition to hBN at about 1800 K in the nitrogen atmosphere [11-12]. During laser heating, cBN transforms to hBN and then hBN gradually decomposes into gaseous nitrogen and gaseous boron at 2400 to 2600 K [13-14], leading to groove formation. Finally crack initiation occurred at the transition zone, primarily due to thermal expansion mismatch stresses of BN phases. The temperature history of laser heating is useful to support the phase changes discussed above and also to predict the phase transformation depth. A Green's function based approach was utilized to estimate the temperature distribution along the depth. The laser was assumed a rectangular heat source. The temperature distribution during heating was obtained by the solution to heat diffusion equations as described [7]. Laser energy absorption by the PCBN at 10.6 μm was modeled, based on the optical absorption spectra of cBN and AlN (constituents of PCBN) [15-16]. The reflectivity is approximated as 0.30, while the absorption coefficient is taken as 133 cm^{-1}. Figure 10 shows the temperature profile obtained for a laser power of 800 W and a speed of 13 mm/s. It predicts a phase transformation depth of 0.5 mm, based on equilibrium 1800 K. However, the experimental data show a depth of 1 mm suggesting phase change can occur under non-equilibrium conditions at lower temperatures. Support for phase change at about 1000 K in non-equilibrium situations is provided [17].

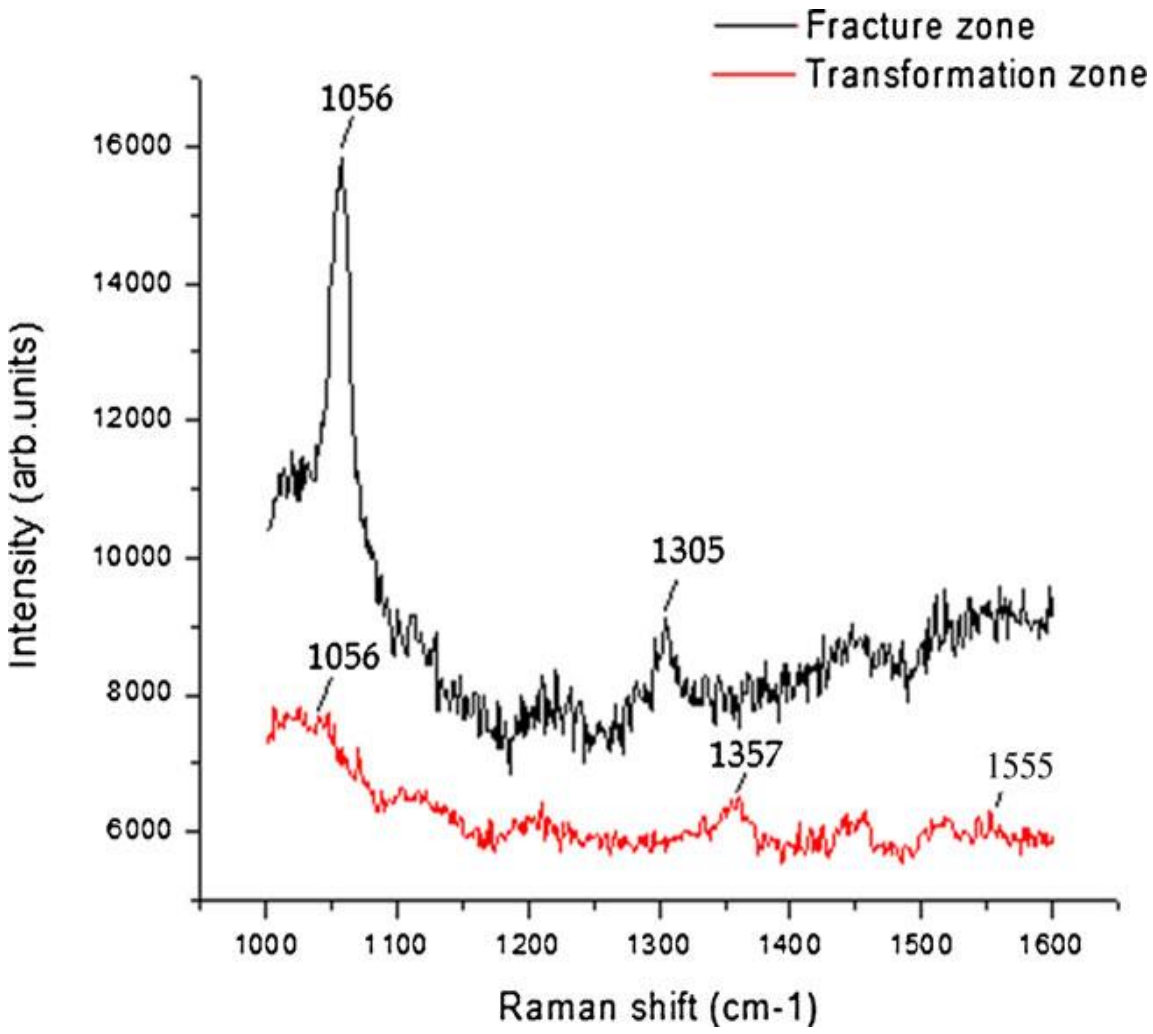

Fig. 9 Raman spectrum of the transformation region in laser cut PCBN with nitrogen gas

Table 5 Raman peaks (cm^{-1}) for various forms of BN

cBN	hBN	rBN	*wBN	eBN
1056 (TO),	1357	790,1370	1015, 1108,	1555-1590
1305 (LO)			1253, 1295	

* It is difficult to obtain good Raman spectra of w-BN because of the powder form

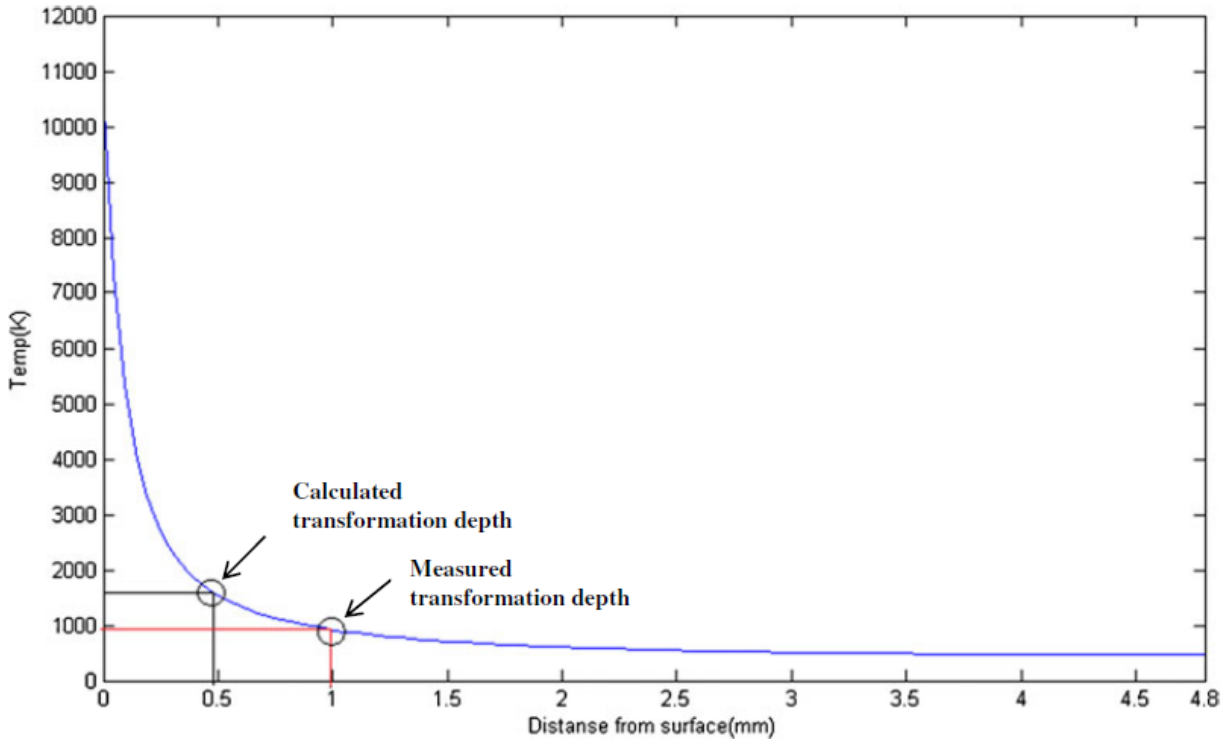

Fig. 10 Surface temperature plot across the thickness for nitrogen-assisted laser cutting (power=800 W, speed=13 mm/s)

To acquire a full understanding of the influence of laser and other process parameters, a 2^3 factorial DOE was pursued and the experimental data were analyzed with JMP® software. Analysis of variance (ANOVA) was then conducted to identify the significance of main and interactions effects for all factors. The objective here was to determine the factors that minimize the transformation depth, R_a, and taper. The three inputs (factors) considered important to the operation are laser power, speed, and gas pressure. The relative importance of each of these factors on each of the responses is ascertained below. The eight different combinations of factors were attempted to establish the best way to cut 4.8 mm thick PCBN.

Table 6 ANOVA results on phase transformation depth of nitrogen-assisted CO_2 laser experiment

Source	Sum of squares	Mean square	DF	F Ratio	P-value
A-laser power	3.43176	3.43176	1	734.3928	<0.0001
B-cutting speed	1.27126	1.27126	1	272.0477	<0.0001
C-gas pressure	0.19141	0.19141	1	40.9608	0.0001
AB	0.09766	0.09766	1	20.8984	0.0013
AC	0.00006	0.00006	1	0.012	0.915
BC	0.04101	0.04101	1	8.7753	0.0016
Error	0.04206	0.00467	9	-	-
Corrected Total	5.35866	-	15	-	-

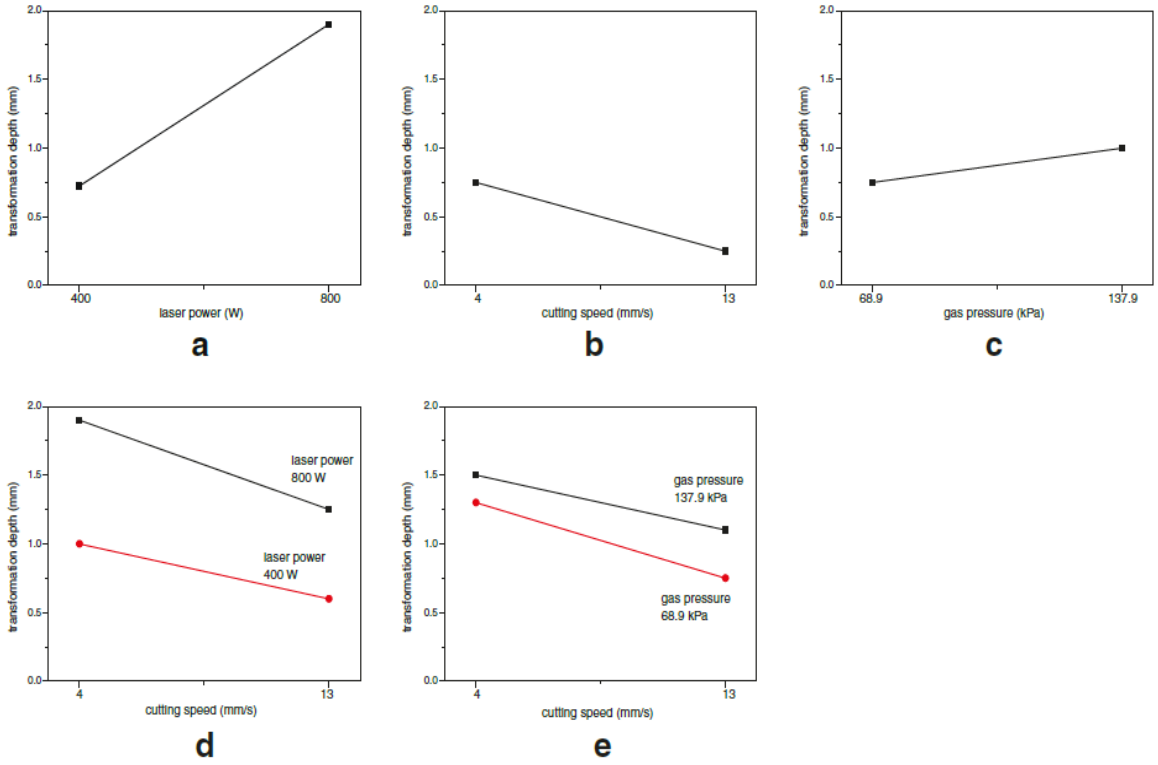

Fig.11 Significant main effects of (a) laser power, (b) cutting speed, and (c) gas pressure and interaction effects of (d) laser power and cutting speed, (e) cutting speed and gas pressure on transformation depth

Table 6 and Figure 11 provide the results on the phase transformation depth. For a confidence level of 95% (α=0.05), all three main effects and two of the three interaction effects (interaction effects between laser power and cutting speed, and between cutting speed and gas pressure) were significant. Transformation depth increases with an increase in laser power and gas pressure, and a decrease in cutting speed. The effects of cutting speed are stronger at high levels of laser power and gas pressure. Ignoring higher-order interactions, a standard model fitted to ANOVA data is given by:

$$\textit{Transformation depth } (\mu m) = 3.082 \times A - 44.273 \times B - 0.087 \times A \times B - 0.326 \times B \times C - 163.347 \quad (1)$$

The results of Eq. (1) also conform to the physical understanding for this process. For instance, when the laser power (A) increased, the depth of transformation ascended. This could be explained by increasingly more energy was injected to promote the phase change from sp^3 cBN to sp^2 phases like hBN.

Table 7 and Figure 12 show the results of significant main and interaction effects of DOE on R_a. Higher-order interaction effects were not significant. Two main effects (power and speed) and one interaction (between power and speed) effect were statistically significant at the significance level of α=0.05. Table 8 and Figure 13 show the results of significant main and interaction effects of DOE on taper rating. Laser power, cutting speed, and interaction between them are found to exhibit the most significant effects.

Table 7 ANOVA results on R_a rating of nitrogen-assisted CO_2 laser experiment

Source	Sum of squares	Mean square	DF	F Ratio	P-value
A-laser power	5.0625	5.0625	1	22.0909	0.0011
B-cutting speed	5.0625	5.0625	1	22.0909	0.0011
C-gas pressure	0.0625	0.0625	1	2.4545	0.1516
AB	14.0625	14.0625	1	61.3636	<0.0001
AC	0.0625	0.0625	1	0.2727	0.6141
BC	0.0625	0.0625	1	0.2727	0.6141
Error	2.0625	0.2292	9	-	-
Corrected Total	26.9375	-	15	-	-

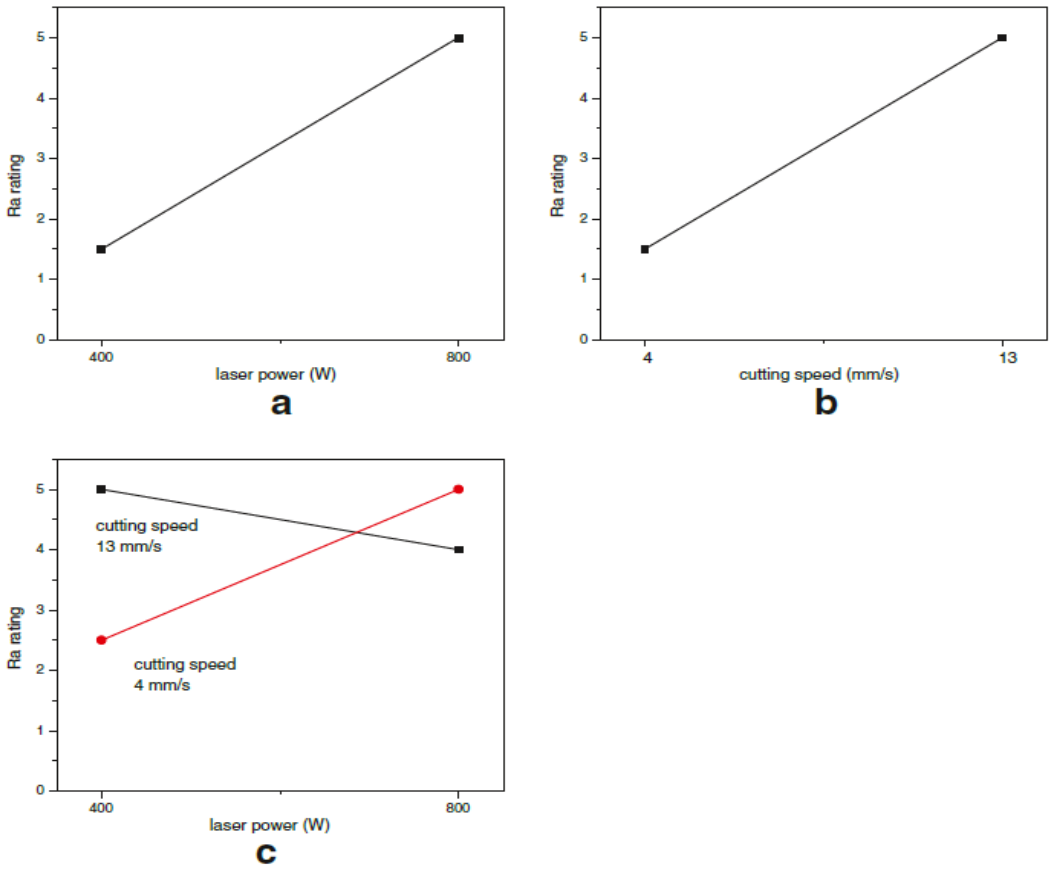

Fig. 12 Significant main effects of (a) laser power, (b) cutting speed and interaction effect (c) laser power and cutting speed on R_a rating

Table 8 ANOVA results on taper rating of nitrogen-assisted CO_2 laser experiment

Source	Sum of squares	Mean square	DF	F Ratio	P-value
A-laser power	3.0625	3.0625	1	25.9412	0.0007
B-cutting speed	3.0625	3.0625	1	25.9412	0.0007
C-gas pressure	0.5625	0.5625	1	4.7647	0.0569
AB	22.5625	22.5625	1	191.1176	<0.0001
AC	0.0625	0.0625	1	0.5294	0.4854
BC	0.0625	0.0625	1	0.5294	0.4854
Error	1.0625	0.1186	9	-	-
Corrected Total	30.4375	-	15	-	-

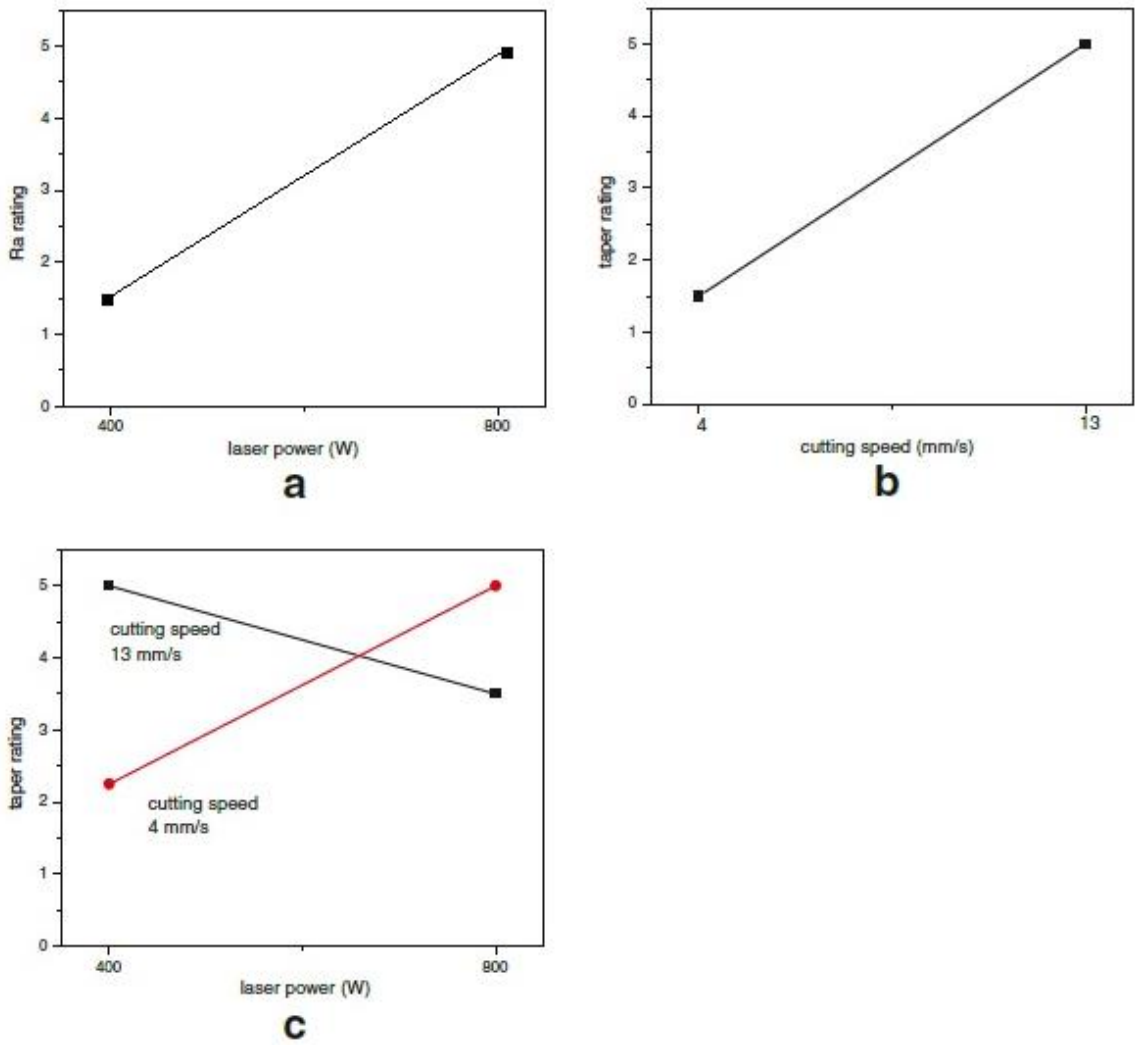

Fig. 13 Significant main effects of (a) laser power, (b) cutting speed and interaction effect (c) laser power and cutting speed on taper rating

2.3.2 Waterjet-assisted CO2 laser cutting

Figure 14 shows a plot of line energy against type of cut. Here line energy is defined as P/V in contrast to the previous case. Threshold energy (P/V) for cutting is 1.33 times higher than that for nitrogen-assisted cutting, which could be explained as follows. When the laser beam impinges on PCBN at a point, groove formation occurs during, as well as after, laser irradiation due to heat conduction. Unlike nitrogen, the succeeding waterjet has a severe cooling effect that can counteract "after laser irradiation" heating effect, limiting the depth of groove and subsequent crack initiation. In addition, the water vapor cloud present in the cutting zone can absorb laser radiation. Thus, more line energy is required to cause cutting for the LWJ case. Another observation in Fig. 14 is it does not cut PCBN in high waterjet pressure (6895 kPa) at the same laser power and speed as in low waterjet pressure (413.7 kPa); this further supports the above hypothesis. Another interesting feature noted is no uncontrolled fracture was determined within the limits of the process parameters investigated.

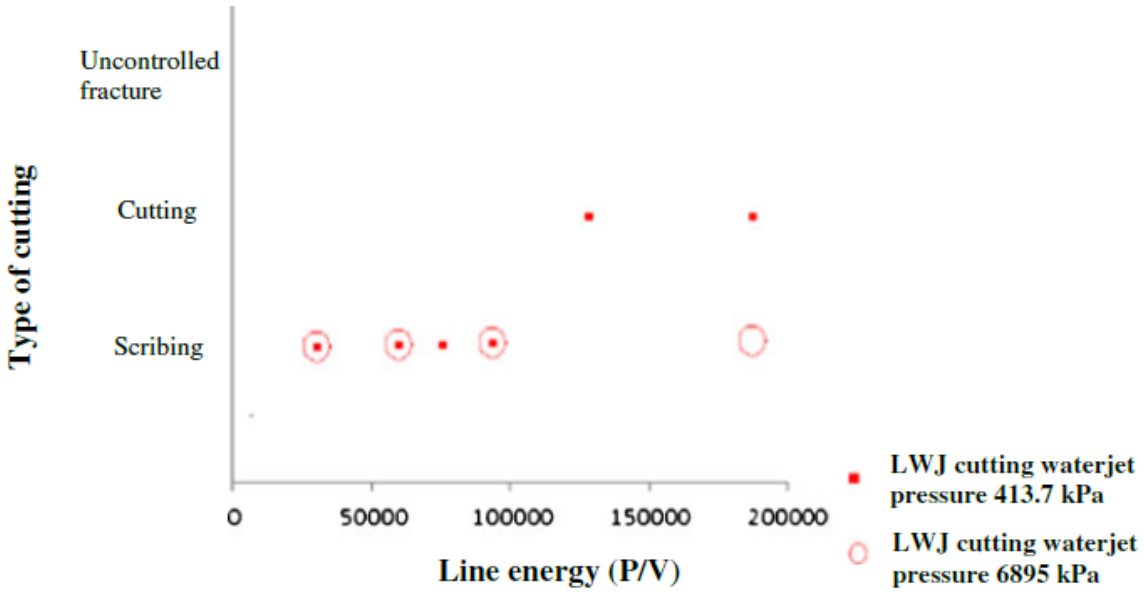

Fig. 14 Effect of line energy on the type of cutting mechanism in LWJ cutting

Figures 15 and 16 show the scanning electron micrographs for the cross sections of through-cut PCBN tool blanks at 4 mm/s (800W, 413.7 kPa) and 6 mm/s (800W, 413.7 kPa), respectively since 13 mm/s was ineffective. Unlike the nitrogen-assisted process, the boundary between the fracture and the phase transformation zone is more horizontal (parallel to the surface). In addition, the fracture zone exhibited a finer structure. Figure 17 shows the Raman spectra of fracture and phase transformation zone. Two peaks (1055 and 1302 cm^{-1}) characteristic of cBN are noted in the fracture zone. On the other hand, two new phases with peaks at 808 and 1355 cm^{-1} are seen in the phase transformation zone, representing boron oxide (B_2O_3) and hBN respectively. Thus, during laser cutting, a series of mechanisms, such as phase transition to hBN, decomposition of hBN to B and N, chemical reaction of boron with water and crack separation, have occurred. Further evidence on the formation of B_2O_3 is the observation of presence of a white glassy layer along the cutting path.

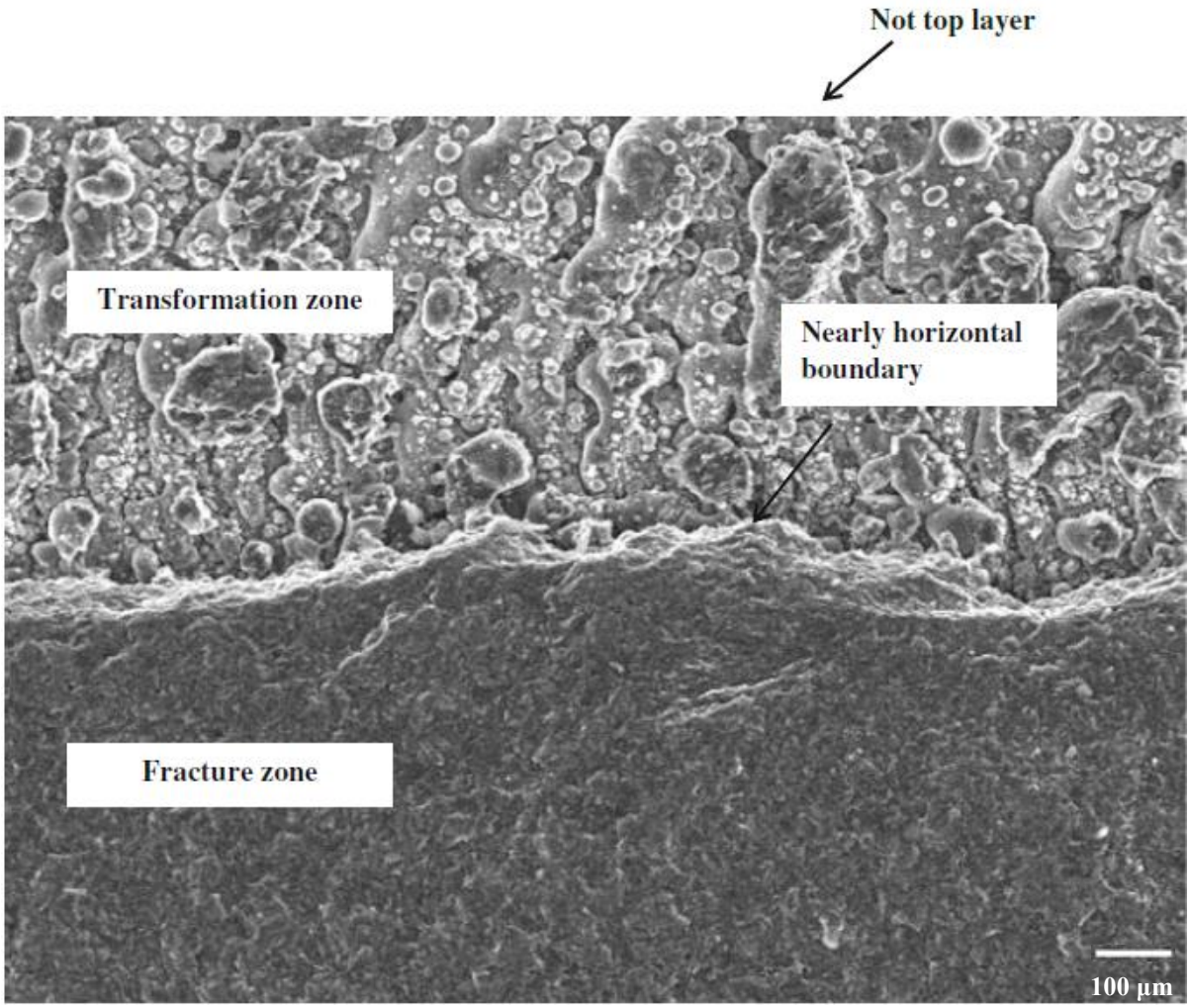

Fig. 15 SEM images of 413.7 kPa waterjet-assisted machined cross section at 800W and 4mm/s (×100)

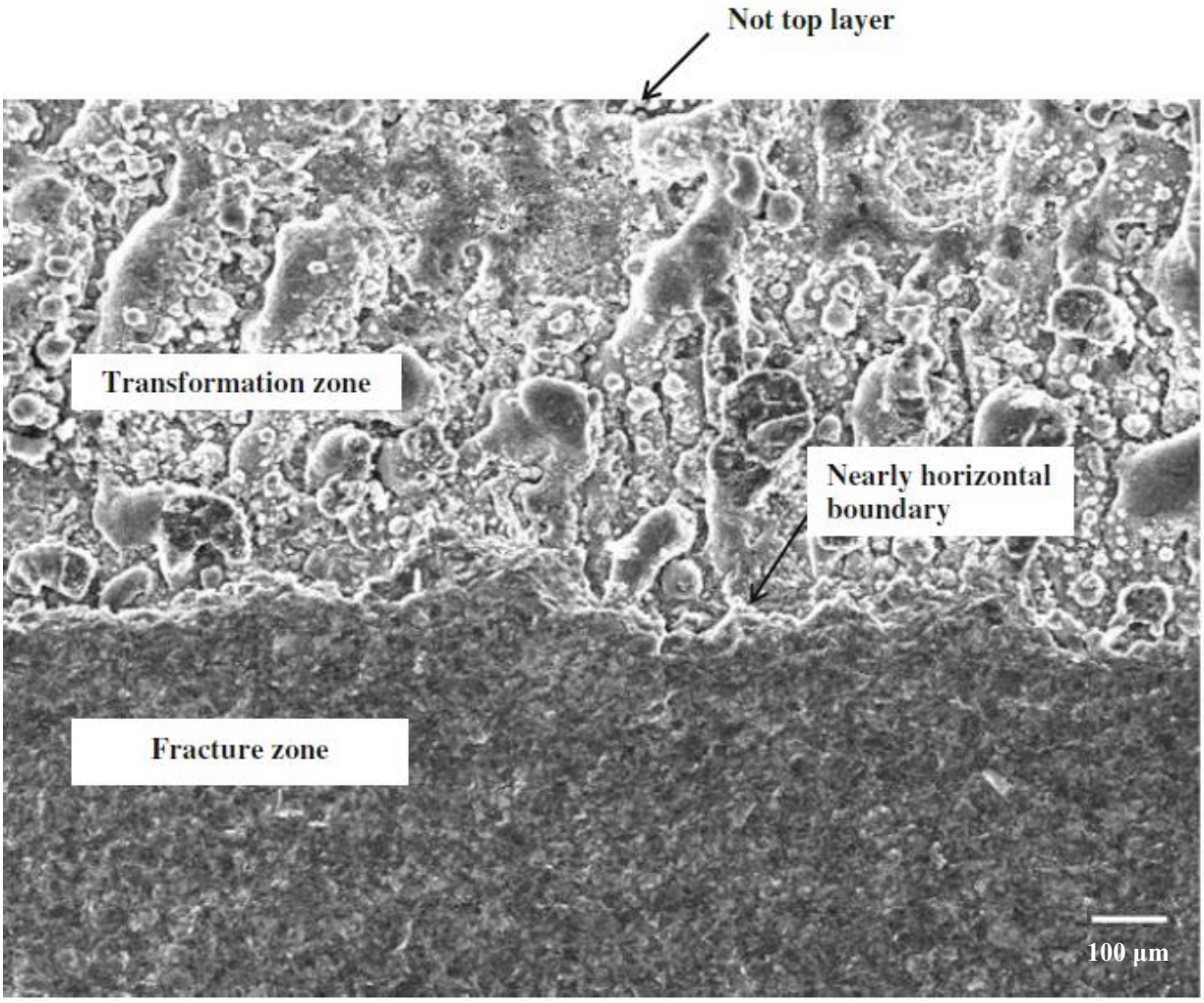

Fig. 16 SEM images of 413.7 kPa waterjet-assisted machined cross section at 800 W and 6mm/s (×100)

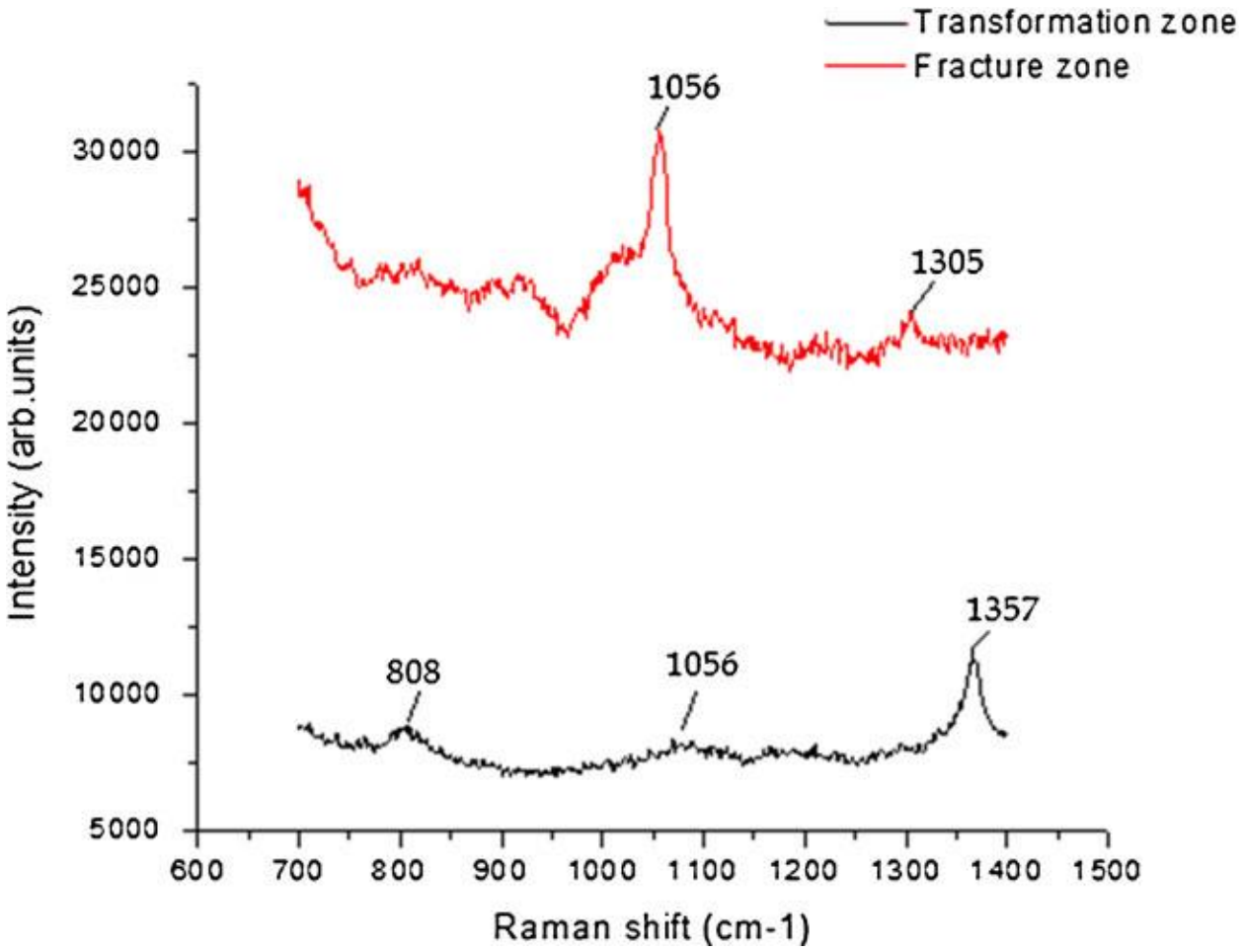

Fig. 17 Raman spectrum of transformation region in LWJ cut PCBN

The factorial DOE results on phase transformation depth are presented in Table 9 and Figure 18. The main effects of laser power and waterjet pressure were significant while the interaction effects are insignificant. A comparison with nitrogen-assisted laser cutting showed smaller phase transformation depth. A standard model can approximate the transformation depth, such as:

$$\textit{Transformation depth } (\mu m) = 1.694 \times A - 0.059 \times C - 126.696 \qquad (2)$$

Table 9 ANOVA results on phase transformation depth of waterjet-assisted CO_2 laser experiment

Source	Sum of squares	Mean square	DF	F Ratio	P-value
A-laser power	0.9180	0.9180	1	606.950	0.0258
B-cutting speed	0.0351	0.0351	1	22.215	0.1303
C-waterjet pressure	0.2926	0.2926	1	193.462	0.0457
AB	0.0406	0.0406	1	26.851	0.1214
AC	0.2346	0.2346	1	155.116	0.0510
BC	0.000013	0.000013	1	0.0083	0.942
Error	0.013608	0.0015	9	-	-
Corrected **Total**	1.5523	-	15	-	-

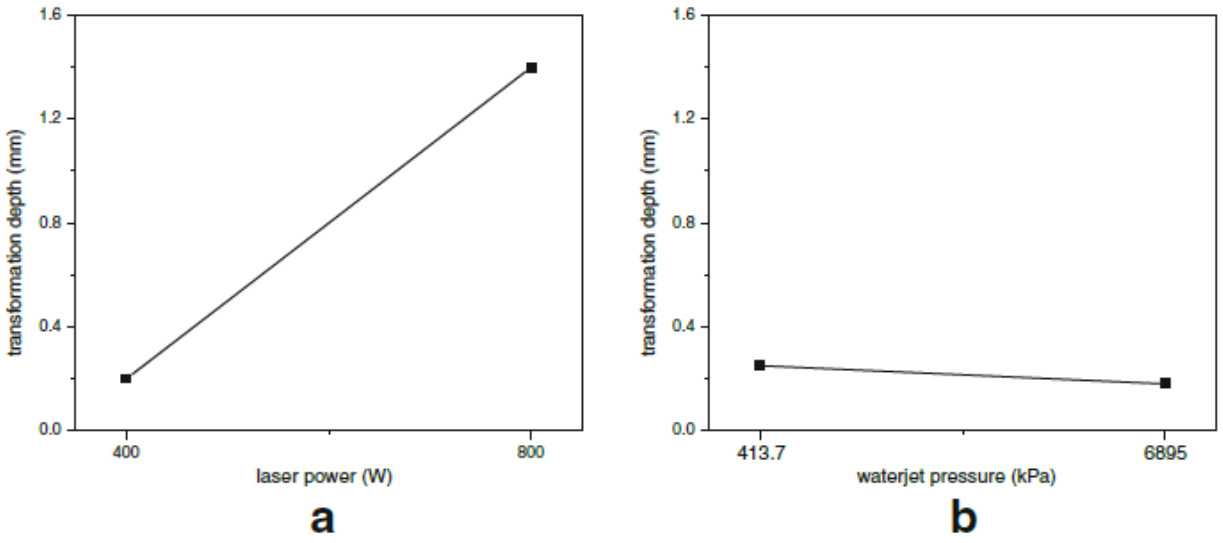

Fig. 18 Significant main effects of (a) laser power and (b) waterjet pressure on transformation depth

Table 10 ANOVA results on R_a rating of waterjet-assisted CO_2 laser experiment

Source	Sum of squares	Mean square	DF	F Ratio	P-value
A-laser power	4	4	1	28.8	0.0005
B-cutting speed	0.25	0.25	1	1.8	0.2126
C-waterjet pressure	4	4	1	28.8	0.0005
AB	0.25	0.25	1	1.8	0.2126
AC	4	4	1	28.8	0.0005
BC	0.25	0.25	1	1.8	0.2126
Error	1.25	0.1389	9	-	-
Corrected Total	14	-	15	-	-

Table 11 ANOVA results on taper rating of waterjet-assisted CO_2 laser experiment

Source	Sum of squares	Mean square	DF	F Ratio	P-value
A-laser power	1.0000	1.0000	1	7.2	0.0251
B-cutting speed	0.2500	0.2500	1	1.8	0.2126
C-waterjet pressure	1.0000	1.0000	1	7.2	0.0251
AB	0.2500	0.2500	1	1.8	0.2126
AC	1.0000	1.0000	1	7.2	0.0251
BC	0.2500	0.2500	1	1.8	0.2126
Error	1.2500	0.1389	9	-	-
Corrected Total	5.0000	-	15	-	-

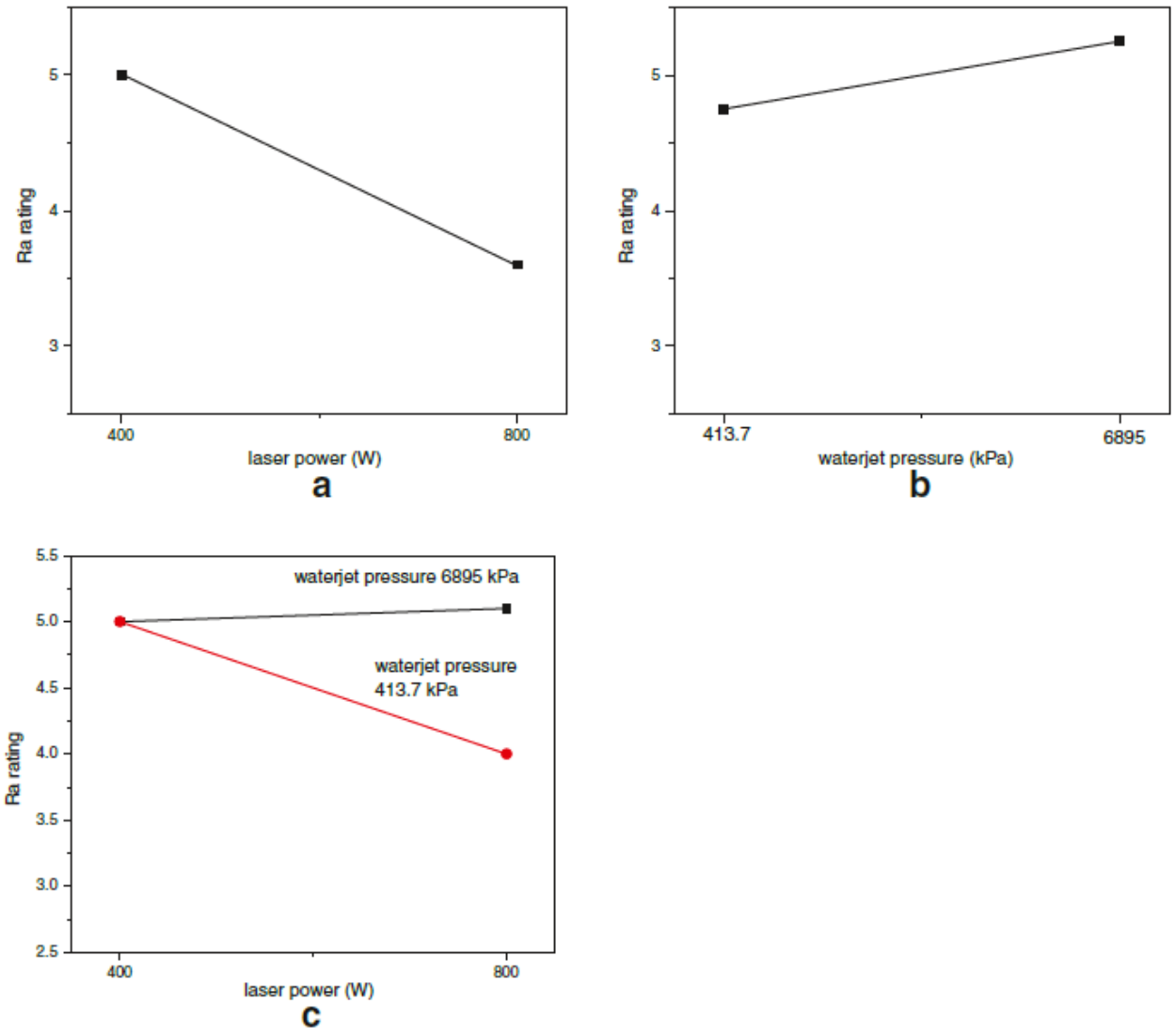

Fig. 19 Significant main effects of (a) laser power, (b) waterjet pressure and interaction effect of (c) laser power and waterjet pressure on R_a rating

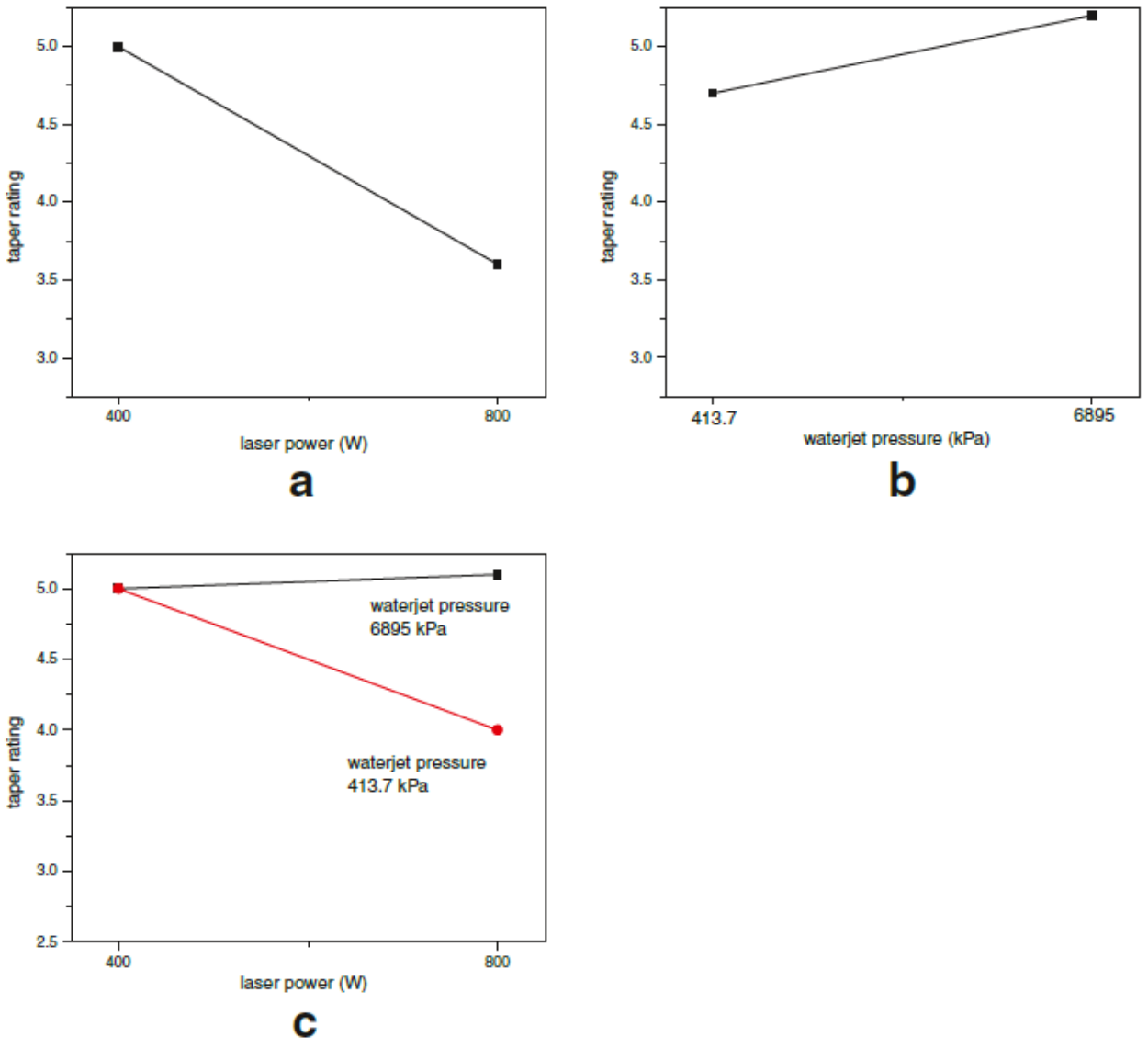

Fig. 20 Significant main effects of (a) laser power, (b) waterjet pressure and interaction effect of (c) laser power and waterjet pressure on taper rating

The factorial DOE results on R_a and taper ratings are presented in Tables 10 and 11 as well as Figures 19 and 20. The main effects (laser power and waterjet pressure) as well as the interaction between laser power and waterjet pressure have statistical significance at the significance level of α=0.05.

2.4 Conclusions

CO_2 laser cutting experiments were conducted on 4.8 mm thick solid PCBN tool blanks with the assistance of nitrogen and waterjet. A 2^3 factorial design of experiments was performed to determine the main effects and interaction effects of laser power, cutting speed, and gas/waterjet pressure on phase transformation depth, R_a, and taper angle. Results showed material removal occurred beginning with the phase transformation of cBN to hBN, followed by the decomposition of hBN and chemical reactions with water, and ending with crack separation. Waterjet improved the cut quality by a smaller phase transformation depth, less taper, and finer fracture zone compared to nitrogen although the latter required less energy for cutting and did not undergo any chemical reaction. The statistical analysis revealed laser power followed by waterjet pressure had the most significant effects among all the factors.

Acknowledgments

This research is based on the financial support by the National Science Foundation award under Grant No. CMMI-1000035. The authors also gratefully acknowledge the polycrystalline boron nitride tool blanks donated by Diamond Innovations, INC, Worthington, OH.

References

1. Wentorf RH (1957) Cubic form of boron nitride. J Chem Phys 26(4):956

2. Ding X, Liew WYH, Liu XD (2005) Evaluation of machining performance of MMC with PCBN and PCD tools. Wear 259(7-12):1225-1234

3. www.ssl-laser.com. Accessed on 21 April 2013

4. http://www.iskydiamond.com/product/01.php?cb_idx=9. Accessed on 21 April 2013

5. http://www.swissphotonics.net/libraries.files/SwissLaserNet_11.09.pdf. Accessed on 21 April 2013

6. Pauchard A, Marco MD, Carron B et al (2008) Recent developments in the cutting of ultra hard materials using water jet-guided laser technology, ALAC conference, Minneapolis

7. Kalyana-sundaram D, Wille J, Shrotriya P, Molian P (2008) Laser/waterjet machining of polycrystalline cubic boron nitride. Transactions of NAMRI/SME, Vol. 131/517-524

8. Melaibari A, Shotriya P and Molian P (2011) Effect of fluid medium on laser machining of polycrystalline cubic boron nitride tool, 44th CIRP conference on manufacturing systems, may 31-June 3, Madison, WI

9. Melaibari A, Molian P, Shrotriya P (2012) Two–dimensional contour cutting of polycrystalline cubic boron nitride using a novel laser/water jet hybrid process. Int J Adv Manuf Technol 62:641-649

10. Wang J, Gu Y, Li Z et al (2013) Growth and optical properties of explosion phase boron nitride octahedron crystals. Am Chem Soc 13(2):599-605

11. Leichtfried G et al (2002) Properties of diamond and cubic boron nitride. In: Beiss P et al Landolt Börnstein – Group VIII Advanced Materials and Technologies: Powder Metallurgy Data. Refractory, Hard and Intermetallic Materials. Springer, Berlin, pp 118-139

12. Liu QX, Yang GW, Zhang JX (2003) Phase transition between cubic-BN and hexagonal BN uponpulsed laser induced liquid-solid interfacial reaction. Chem Phys Lett 373(1-2):56-61

13. Barin I (1996) Thermochemical data of pure substances. 3rd edn. VCH, New York, pp 104-121

14. Dreger LH, Dadape VV, Margrave JL (1962) Sublimation and decomposition studies on boron nitride and aluminum nitride. J Phys Chem 66(8):1556-1559

15. Gielisse PJ, Mitra SS, Plendl JN et al (1967) Lattice infrared spectra of boron nitride and boron monphosphide. Phys Rev 155(3):1039-1046

16. Akasaki I, Hashimoto M (1967) Infrared lattice vibration of vapour-grown AlN. Sol State Commun 5, 11:851-853

17. Sachdev H, Haubner H, Noth H, Lux B (1997) Investigation of the c-BN/h-BN phase transformation at normal pressure. Diam Relat Mater 6(2-4):28

CHAPTER 3

NOVEL CRACK SEPARATION MECHANISM IN TWO-DIMENSIONAL CO2 LASER MACHINING THICK POLYCRYSTALLINE CUBIC BORON NITRIDE

A paper prepared for International Journal of Machine Tools and Manufacture

Yixian Wang, Pal Molian and Pranav Shrotriya

Abstract

Polycrystalline Cubic Boron Nitride (PCBN) is widely utilized in material removal operations but difficult-to-machine material for almost 40 years, which is fabricated by state-of-the-art techniques such as wire EDM and Nd:YAG laser, restricted by slow material removal rate and poor cut quality. Our group previously used a hybrid CO_2 Laser/Waterjet (CO_2-LWJ) that performed well when machining PCBN in one and two dimensions with limited thickness (no more than 1.6 mm). A superior controlled crack separation mechanism was explored in two-dimensional cutting 4.8 mm thick PCBN tools in solid form. Both laser alone and LWJ methods with nitrogen as an assist gas examined and successful in performing a 120 ˚ contour cut. Both the phase transition zone and fracture zone were characterized and analyzed by means of scanning electron microscopy (SEM), energy dispersive X-ray spectroscopy (EDS), Raman spectroscopy and optical profilometer. A finite element analysis (FEA) computed stress field was compared with surface profiles measured by a surface profilometer. Fracture energy release rate based upon phase change from sp^3 cubic Boron Nitride (cBN) to sp^2-bonded structure such as hexagonal Boron Nitride (hBN) was calculated in order to predict the fracture behaviors. Superior cut quality in terms of controlled cracking path, surface roughness, taper angle was

observed in LWJ in contrast of laser alone method and the phenomena was also fully explained by a crack path stability model.

KEYWORDS: Cubic boron nitride; Two-dimensional cutting; CO_2 laser; Waterjet; Controlled crack separation mechanism

3.1 Introduction

Polycrystalline Cubic Boron Nitride (PCBN) is one of the most demanding tooling materials due to its superb hardness, resistance to plastic deformation, abrasive and thermal shock resistance. For example, it is an obvious choice for machining hardened ferrous material because of its exceptional heat resistance (retains constant hardness at elevated temperature), sufficient toughness and chemical stability (inert to metals such as iron and titanium). PCBN homogeneous blanks are synthesized from cubic boron nitride whose hardness is only excelled by diamond and metallic binders such as Co or ceramic binders such as AlN and TiN under extreme high temperatures (1300-1600 ˚C) and high pressures (4-6 GPa)[1].

PCBN tool blanks are usually machined into three different forms: baked full-face form and brazed form by depositing sintered layer on tungsten carbide; solid form which is self-supported. The first two forms require less PCBN materials and possess composite properties. The inserts in solid form provide two available sides for double-edge cutting and are used for drawing dies. The tool inserts in the thickness such as 1.6 mm, 3.2 mm and 4.8 mm, are available as index geometries such as round, triangle, square and rhombus to fit standard negative rake tool holders. The most common angles of rhombic tools include 35 ˚, 55 ˚ and 80 ˚.

The super-high hardness, thermal and chemical inertness limit the manufacturing of PCBN tool inserts. Currently used methods include diamond sawing, electric discharge machining (EDM), and conventional Nd:YAG laser. However, all of them suffer from

deficiencies such as low cutting speed and cut quality and required post treatment. Swiss Federal Institute of Technology Lausanne established a hybrid technique called Laser Microjet® (LMJ®), which combines the pulsed Nd:YAG laser with water[2]. LMJ® succeeded to cut 4.8 mm pure CBN into different custom shapes at the speed of 6-6.85 mm/min with 70-90 passes[3]. However, LMJ® still suffers from a slow machining rate due to the multiple passes.

Lumely[4] first attempted to separate brittle material such as alumina with a single CO_2 laser. The crack propagation followed the beam path and the energy consumption was much less than the standard method. Tsai and Chen[5] established an approach using a dual laser, one is focused to generate a groove and the other to generate tensile stress to guide the crack propagate through the thickness. Curved lines and a right angle were performed successfully on the thick alumina substrate. Our group developed a hybrid technique called CO_2-Laser/Waterjet (CO_2-LWJ) to cut PCBN both in one and two dimensions. Previously obtuse angles (120 ˚ and 135 ˚) were performed successfully on both the solid-form and full-face form of 1.6 mm thickness[6]. Thick PCBN tool blanks (4.8 mm) were cut through in one dimension with both nitrogen and LWJ[7].

In this paper, we explored an improved technique utilizing waterjet plus nitrogen as assist gas to cut thick PCBN in solid form at 90 ˚ and 120 ˚ angle. Cut quality including phase transformation depth, surface roughness and taper were characterized and the transiting process was examined. The controlled crack separation mechanism was also examined based upon formulated FEM models to help predict the cutting characteristics and fracture energy.

3.2 Experimental details

3.2.1 Material

Experiments conducted on electrically insulating PCBN tool blanks (BZN 7000S, Diamond Innovations, Inc., Worthington, OH) with average grain size of 15 μm, The sample is 4.8-mm-thick in solid form, composed of 82% cBN and 18% secondary ceramic binder phase such as AlN and other impurities including aluminum boride. The Ra of BZN 7000S on the polished facade and on the side is 0.3 and 3 μm, respectively.

3.2.2 Experimental methods

The CO_2-Laser/Waterjet (CO_2-LWJ) system, schematically shown in Fig. 1, is comprised of a continuous CO_2 laser, a computer numerical controller (CNC), an X-Y positioning table, a water pump, assist gas bottles and a unique laser head. All experiments were carried out by a continuous wave, 10.6 μm CO_2 laser at rated power of 1.5 kW. The laser beam was launched through a circular polarizer and then transmitted on a 127-mm (5-in) focal length lens. The spot size of the focus beam is 0.2 mm. Both laser and assist gas went coaxially through a brass nozzle with a 1 mm diameter orifice. The beam was focused on the PCBN sample, which was mounted on an X-Y positioning, by setting the standoff spacing between specimen surface and nozzle at 1 to 2 mm.

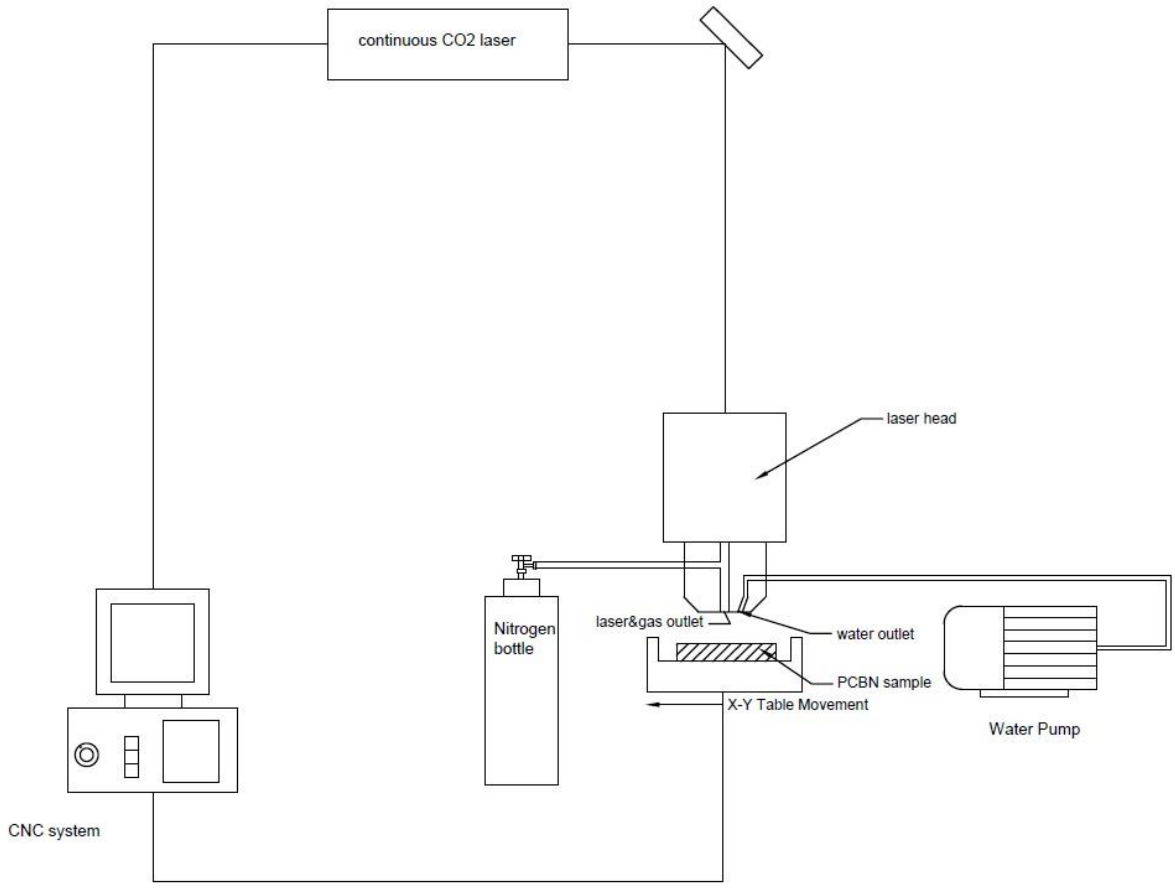

Fig. 1 Schematic presentation of CO_2-Laser/Waterjet system

Two sets of two-dimensional (2D) cutting experiments were conducted in total. The first set of experiments was carried out by a laser alone with nitrogen at pressure of 68.9 kPa (10 psi) as the assist gas. The second set of experiments was performed by combining LWJ with 34.5 kPa (5 psi) nitrogen as an assist gas to identify the combination effect of nitrogen and water quenching. It is shown from Figure 1 that the LWJ nozzle contained two outlets: one is for both laser and assist gas and the other is for a low-pressure waterjet at 413.7 kPa (60 psi). The spacing between the two holes is 6 mm in order to prevent the direct interaction of laser beam and water. Table 1 shows the main parameters used in both sets of experiments.

Table 1 Main parameters of 2D experiment

Experimental methods	Laser power (W)	Cutting speed (mm/s)	Line energy P/v (kJ/m)
N_2-assisted laser alone	400	4.23	94.5
Air-assisted LWJ	850	4.23	200.9
N_2-assisted LWJ	850	4.23	200.9

Two sets of one-dimensional (1D) cutting experiments were conducted to establish a finite element model to simulate and predict the dimensions of the phase transformation zone based upon expansion strain compared with measured surface profiles by phase transformation. The main parameters used in the trials are shown in Table 2.

Table 2 Main parameters of 1D experiment

Experimental methods	Laser power (W)	Cutting speed (mm/s)	Line energy P/v (kJ/m)
N_2-assisted laser alone	400	4.23	94.5
	400	6.35	63.0
Air-assisted LWJ	800	6.35	126.0
	800	8.46	94.5

3.2.3 Characterization and analysis

An optical profilometer (Zygo NewView 7100) with 5× and 20× magnifications was utilized to measure and analyze the kerf profile, taper angle and surface roughness etc. An optical microscope (Eclipse E-600FN, Nikon Inc., resolution = 1 μm) was used to measure both the width of groove and Heat Affected Zone (HAZ), and the depth of groove with the aid of a remote focus accessory (600FN, Nikon Inc.). A scanning electron microscope (SEM Model JOEL JSM-606LV at 20 kV) was used to characterize the microstructure and topography such as transformation depth and analyze the phase transformation and crack propagation regions before and after turn. Energy Dispersive X-ray Spectroscope (SEM FEI Quanta FEG 250 at 10 kV) was used to acquire the element mapping in the phase transformation and crack propagation regions. A Raman visual spectroscope (Renishaw-inVia Raman Microscopy) with a wavelength of 532 nm and power of 4 mW was utilized to identify the phase signatures ranging from 200 to 1800 cm^{-1}.

3.3 Numerical modeling

3.3.1 FEA simulation of phase transformation induced deformation and stress field

Finite element analysis (FEA) was utilized to simulate and predict the surface profiles that underwent phase transformation induced expansion, in order to compare them with the measured deformation results. It is hypothesized that the laser irradiated the workpiece and the transition from cBN to hBN took place, consequently leading to volumetric expansion due to phase transition (sp^3-bonded phase to sp^2-bonded phase). The volumetric mismatch in the transformation region then generated a tensile stress field that initiated the crack tip and propagated it in the thickness direction. Deformation induced by phase transformation could be

measured by optical profilometer and validated with the simulation results from numerical modeling. The schematic of phase transformation induced crack propagation is presented in Figure 2.

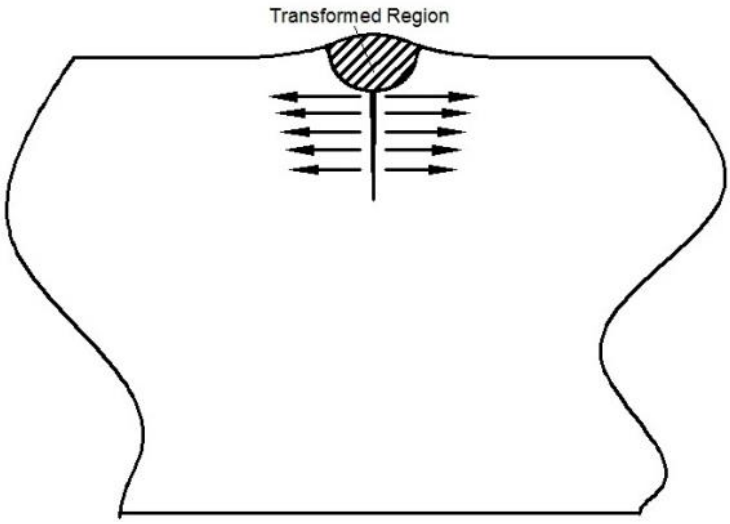

Fig. 2 Hypothesis for phase transformation induced crack propagation

The ABAQUS package (Simulia, Providence, RI) was utilized to formulate the finite element model and predict the possible expansion stress field along the phase transformation region. A half sample based model was formulated due to the symmetry to determine the plane strain deformation in both laser alone and LWJ conditions. Thermal effect is neglected because the temperature stress is much smaller due to high thermal conductivity of PCBN compared to the phase transformation stress. To simplify, we assumed the irradiated region transformed entirely from homogeneous sp^3 cBN to sp^2 hBN. The governing properties of cBN and hBN are shown in Table 3 and used to input in the model. As shown in Figure 2, the transformation region is modeled as a semi-ellipse according to the Gaussian profile of the CO_2 laser beam. The fixed boundary condition along the vertical direction is simulated as the fixture used in the experiment. The dimension of workpiece is 10 mm, considerably larger than the cutting path.

The FEA model is composed of eight-noded quadratic modified axis-symmetric elements. The model partitioned the cutting edge in the perpendicular direction and the mesh was refined until the computed stress was independent of the mesh size. Numerical simulation was performed in two steps for both laser alone and LWJ. The first step used the transformation depth of through-cut case measured from SEM to find the best fit with the experimental measurements and estimate corresponding parameters such as width and expansion strain. In the second step the approximate transformation depth was computed for the scribing case in order to match the experimental measurements based on the surface profiles.

Table 3 Properties of cBN and hBN

Phase of BN	**Density (kg/m^3)**	**Young's modulus (GPa)**	**Poisson ratio**	**Fracture toughness (MPa$\sqrt{m}$)**
cBN	3400	710	0.15	5-7.7
hBN	2010	70	0.2	-

3.3.2 Crack propagation analysis based upon fracture mechanics

Crack propagation behavior of CO_2 laser cutting PCBN could be regarded as a three-dimensional channeling crack initiating from the edge, including two kinds of crack: (1) plane strain crack; (2) channeling crack (See Figure 3). A continuous laser beam started to irradiate from outside the sample edge, initiating a crack tip as a plane strain crack. It is assumed that the plane strain crack could extend along the beam path at a fixed crack depth and constant tip shape in a steady crack growth state. Thus, the driving force for controlled propagation of the crack is determined by the Griffith critical energy release rate at the crack front depth.

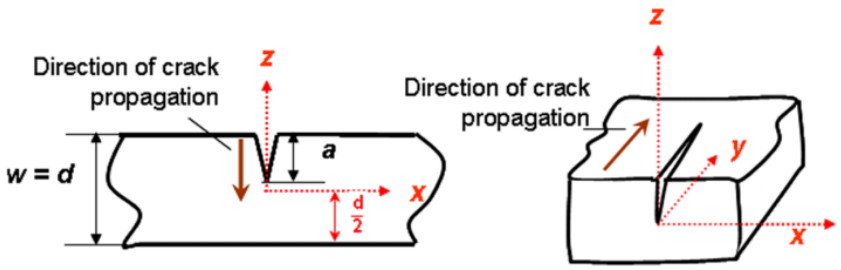

(a) (b)

Fig. 3 (a): plane strain crack; (b): channeling crack

The energy release rate for a channeling crack at different crack depths was calculated by the following procedures. First energy release rate in a plane strain crack was computed based upon the J-integral method in mode I loading using the ABAQUS package. PCBN is super brittle, which could be treated as a linear elastic material. Thus, the J-integral is equal to plane energy release rate and was computed as:

$$J = G_p(a') = \frac{[k_I(a')]^2}{E'} \tag{1}$$

Where $G_p(a')$ and $k_I(a')$ are the energy release rate and stress intensity factor for specific crack length a', respectively. E' refers to the plane strain modulus and $E' = \frac{E}{(1-\nu^2)}$. Therefore, the energy release rate of channeling crack was computed by:

$$G_c = \frac{1}{a}\int_0^a G_p(a')\,da' \tag{2}$$

3.4 Results and discussion

3.4.1 Experimental and quality results

In laser alone cutting experiment, a focused laser beam at line energy of 94.6 kJ/m made a through 120 ˚ angle cut with one single pass. The input line energy is the same as that for the straight line cut. However, the crack trajectory deviated from the laser beam path and attempted

to make a shorter path around the corner. The lagging distance at the turning point measured by an optical microscope was approximately 2 mm. Figure 4 shows the crack trajectory in the backside which did not follow the laser beam path at the top. However, the trial of cutting 90 ˚ with the same parameter merely generated a shallow groove. The crack did not propagate through the thickness since there was not enough thermal stress to break apart the sample. The depth of groove measured was roughly 150 µm before and after the turn.

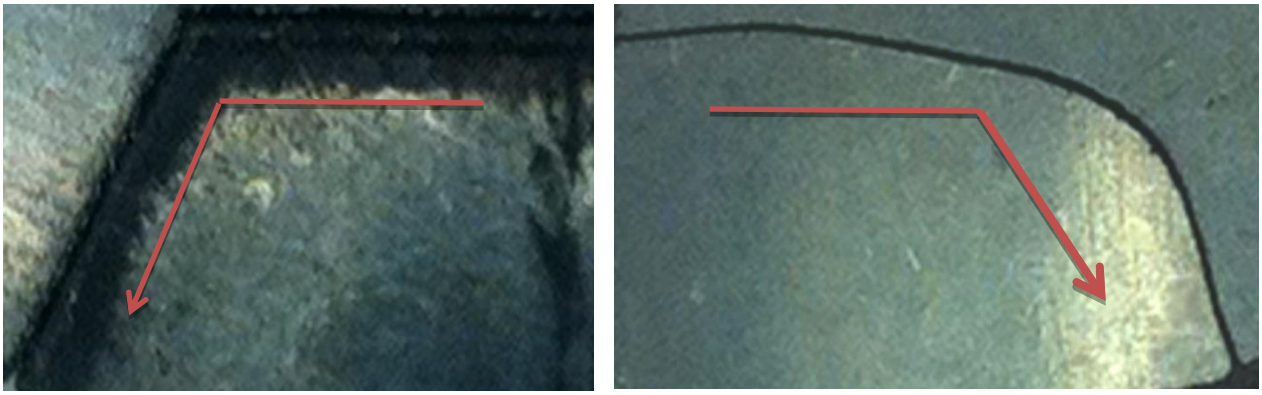

Fig. 4 Photographs of cutting trajectory on both top and bottom surface underwent laser alone and LWJ machining (arrows show the direction of 2D cutting)

In the air-assisted LWJ cutting, the attempt to cut 120 ˚ with a single focused beam was unsuccessful. It was still unreachable even after multiple passes of defocused beam. Spalling cracks began to generate along the groove path, however not reach the threshold value for snapping along the whole thickness. Same results were found for the right angel cut by virtue of LWJ machining.

In the nitrogen-assisted LWJ cutting, a single focused laser beam at line energy of 200.9 kJ/m only scribed the sample. Water possesses a high absorption rate of CO_2 laser energy [], leaving a groove with limited crack propagation in the third direction. In order to help break through the sample, a defocused beam with the same parameter except larger spot size (0.5 mm)

was introduced to cut through. Three defocused-mode passes were utilized to cut through the PCBN sample with negligible surface damage such as lateral or spalling cracking. Based upon our previous experimentation and analysis, the defocused beam enlarged the phase transition region around the groove. Grove depth increased vertically leading to more expansion stress and in turn propagated the crack.

The crack trajectory almost followed the laser beam path within control, especially at the corner of the turning point. Figure 5 shows the cutting trajectory on both the top and bottom surface for a specimen that underwent LWJ machining. It should be noted that there was less laser energy input into the cutting because some energy was absorbed by the water. Yang and Chandar[9] observed and studied the transition from straight to oscillatory crack growth of a thermally quenched glass flask at a dramatic temperature jump. In contrast, a lower temperature gradient induced less driving force, which stabilized the crack separation in control. The formulated model of crack path stability based upon Cotterell and Rice's theory[8] can be utilized to explain this phenomena.

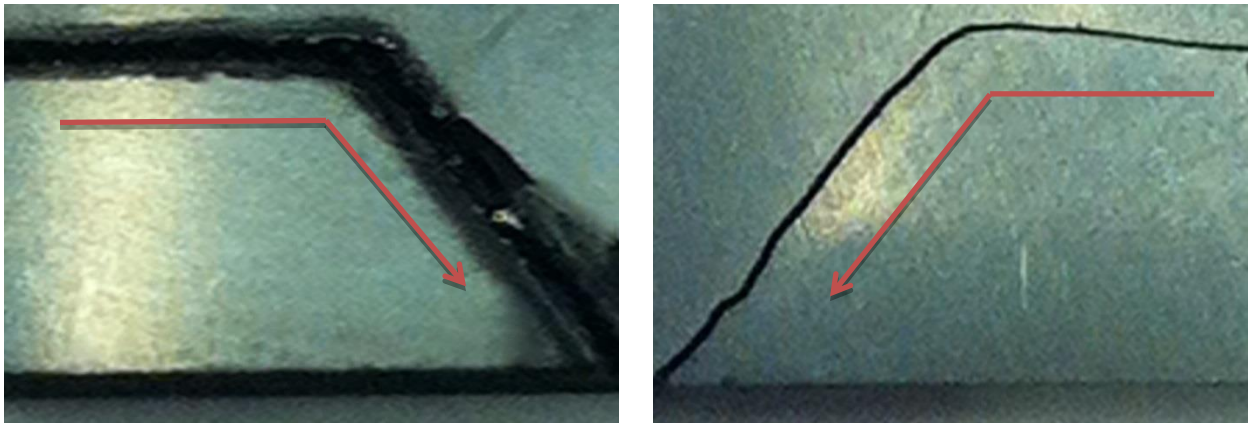

Fig. 5 Photographs of cutting trajectory on both top (left) and bottom (right) surface underwent LWJ machining (arrows show the direction of cutting)

Surface roughness and taper angle of through-cut samples were measured using an optical profilometer. The surface roughness, including arithmetic average (Ra) and root mean

square (RMS), of both transformation zone and fracture zone was measured. It may be noted that the surface roughness either before or after the turn was almost equal and hence only one set of values was examined. The taper angle was measured both before and after the turning point. The cut quality of LWJ is better compared to laser alone with respect to surface roughness and taper angle as shown in Table 4.

Average surface roughness in the transformation region shows that LWJ machining is better than laser alone, mostly owing to oxidation and recast layer prevention by water cooling effect. Average surface roughness in the fracture region of both methods shows no noticeable difference between the two methods due to no phase transition. Taper angle results also indicate the superiority of LWJ techniques, either before or after the turn. The reason was explored before in the crack path stability model.

Table 4 Cut quality of LWJ versus laser alone machining PCBN tool blanks

Methods	**Line energy (kJ/m)**	**Ra (μm)**	**RMS (μm)**	**Taper angle (degree)**
laser alone machining	94.6	Transformation zone: 11.6	Transformation zone: 13.7	Before turn: 12
		Fracture zone: 4	Fracture zone: 5	After turn: 8
LWJ machining	200.9	Transformation zone: 8	Transformation zone: 9.9	Before turn: 4.1
		Fracture zone: 4	Fracture zone: 5	After turn: 4.9

3.4.2 Effect of assisted fluid media

To understand the mechanism of the contour cutting in two dimensions, the transverse sections of both laser alone and LWJ cutting along the beam path was investigated. Scanning electron microscope was taken for three different representative points: (1) after the turn; (2) at the turning point; and (3) before the turn.

Figure 6 shows SEM images of the laser alone machined sample. Two regions with a non-uniform boundary could be distinguished in all images: the shallow machined region near the top surface resulted from phase transformation and chemical reaction; the lower fracture region due to crack initiation and propagation. The microstructures and features were also different before and after the turn. Depths of the transformation region before and after the turning point are approximately 1050 μm and 1000 μm, respectively. Before the turn, recast layer formation resulted in zigzag profiles along the cutting surface. There are minor cracks generating at the transformation region of the turning point. The formation of minor cracks is due to the mismatch of stress fields in the transformation and fracture regions. After the turn, the surface became smoother and depth of transformation was lower than before because the high laser power input led to material evaporation directly rather than melting within a short time.

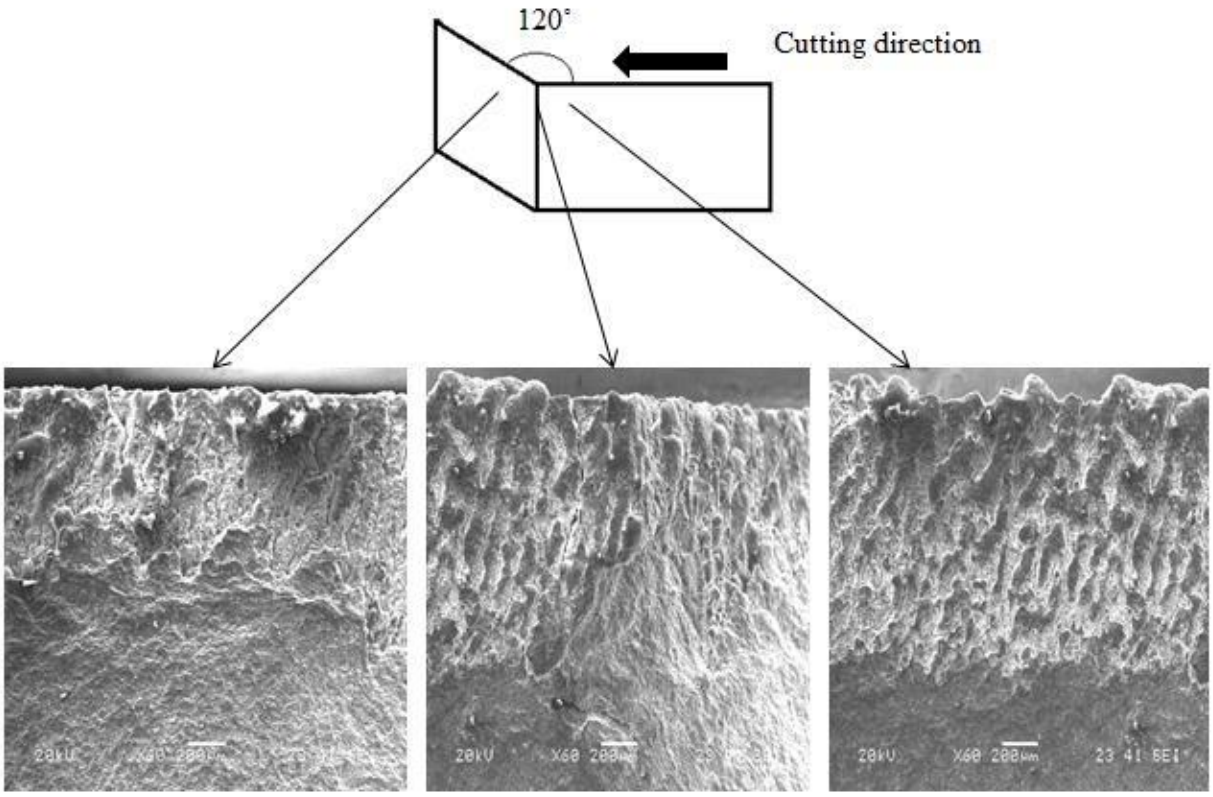

Fig. 6 SEM images of transverse section of laser alone machined sample after the turn (left), at the turning point (middle) and before the turn (right)

Figure 7 shows SEM images of transverse section of LWJ cut samples. There are different microstructures and topography before and after the turn. Unlike laser alone machining, the depth of phase transformation region increase from 750 μm to 1000 μm after passing the 120 ˚ angle. Voids exist in the transformation region both before and after the turn. This can be attributed to the severe quenching effect of water, consequently leading to the evaporation bubbles not escaping to the environment. No obvious minor cracks are observed at the turning point.

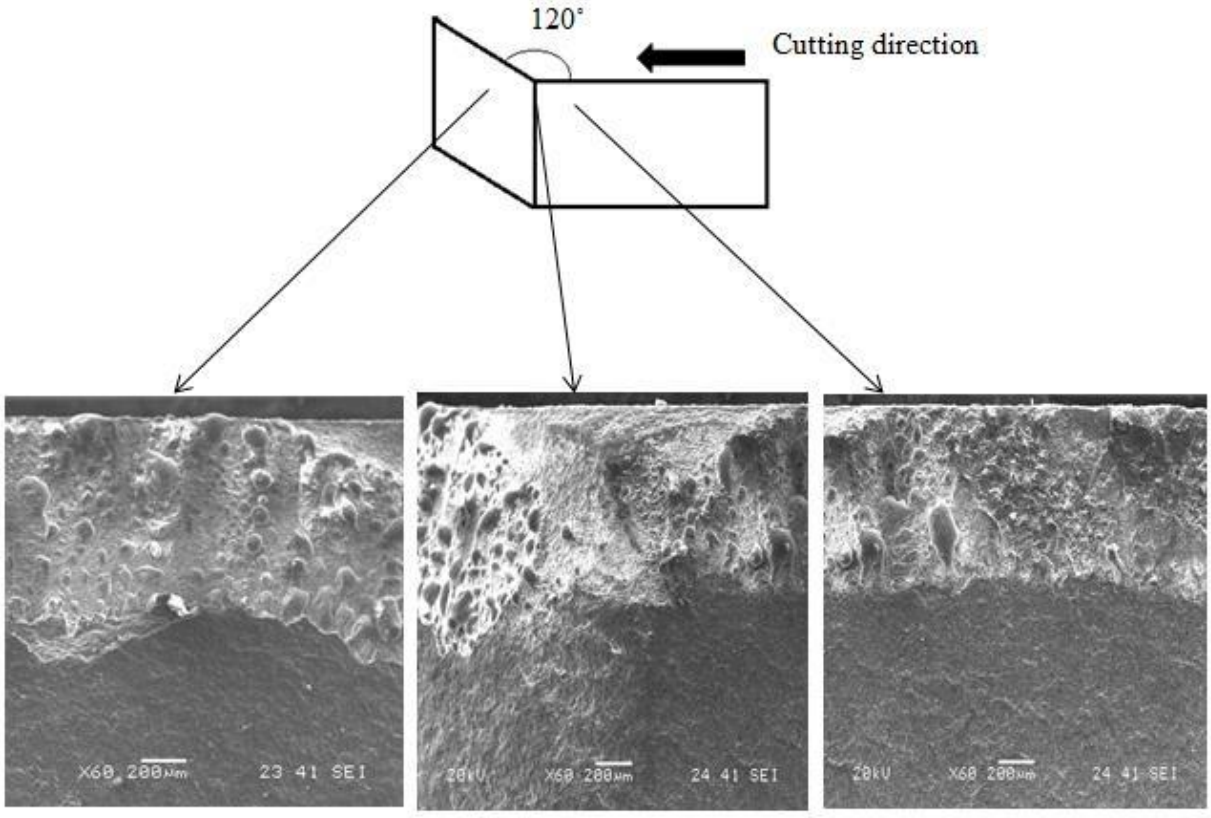

Fig. 7 SEM images of transverse sections of LWJ machined sample after the turn (left), at the turning point (middle) and before the turn (right)

In order to identify the chemical compositions around the cut surface to understand the reactions happened during the process, EDS was conducted to acquire element mapping for the transverse section for through-cut samples that underwent laser alone cutting.

Figure 8(a) shows the secondary image of the transverse section of laser alone cutting at the turning point (corresponds to Figure 5). Figures 8(b)-(e) represent the contour maps of three main elements (B, N and Al). It could be noted that Al largely presents in the transformation region. Possible formation of aluminum oxide in the transformation region was also confirmed by X-ray photoelectron spectroscopy (XPS) in our previous study[10]. Whilst little B or N was found on the surface of the transformation area. The presence of aluminum oxide indicated the

oxidation of binders (AlN) other than the bulk material (BN). It should be mentioned that aluminum oxide possesses 2.4 times to 3.1 times as high a volume as AlN depending on the lattice size of AlN[11, 12]. The volumetric mismatch of AlN and aluminum oxide was also in agreement with the crack separation mechanism. In contrast, the fracture region shows mainly B and N elements, representing the existence of boron nitride (BN) as the as-received material.

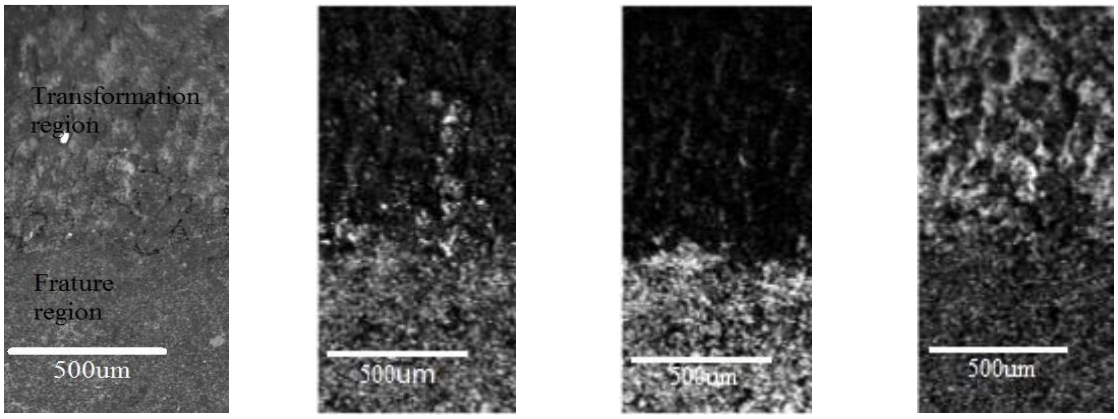

(a) (b) (c) (d)

Fig. 8 (a) SEM image of transverse section of laser alone cutting at the turning point and (b)-(d) shows element mapping of B, N and Al (bright dots show presence of elements based upon the intensity of X-ray)

Figure 9 shows the Raman spectra taken from the transverse sections of both nitrogen-assisted laser and LWJ, including both phase transformation and fracture regions. The fracture zone has two peaks at 1053 and 1304 cm^{-1}, evolving from cBN in TO and LO. These two peaks downshift from the values corresponding to the cBN in single crystalline form, which representatively possesses 1056 cm^{-1} (TO) and 1305 cm^{-1} (LO), respectively. The downshift of peaks could be due to grain size, binders, impurities, residual stress and plastic deformation extent. It is hypothesized that no phase transformation took place in the fracture region due to the

same phase signatures in as-received material. In the phase transformation region, two new phases with different peaks (1361 and 1562 cm^{-1}) are seen. The 1361 cm^{-1} peak corresponded to the hBN phase, which typically possesses a 1366 cm^{-1} peak. The existence of cBN demonstrated the transformation between sp^3 to sp^2 phase in phase transformation region.

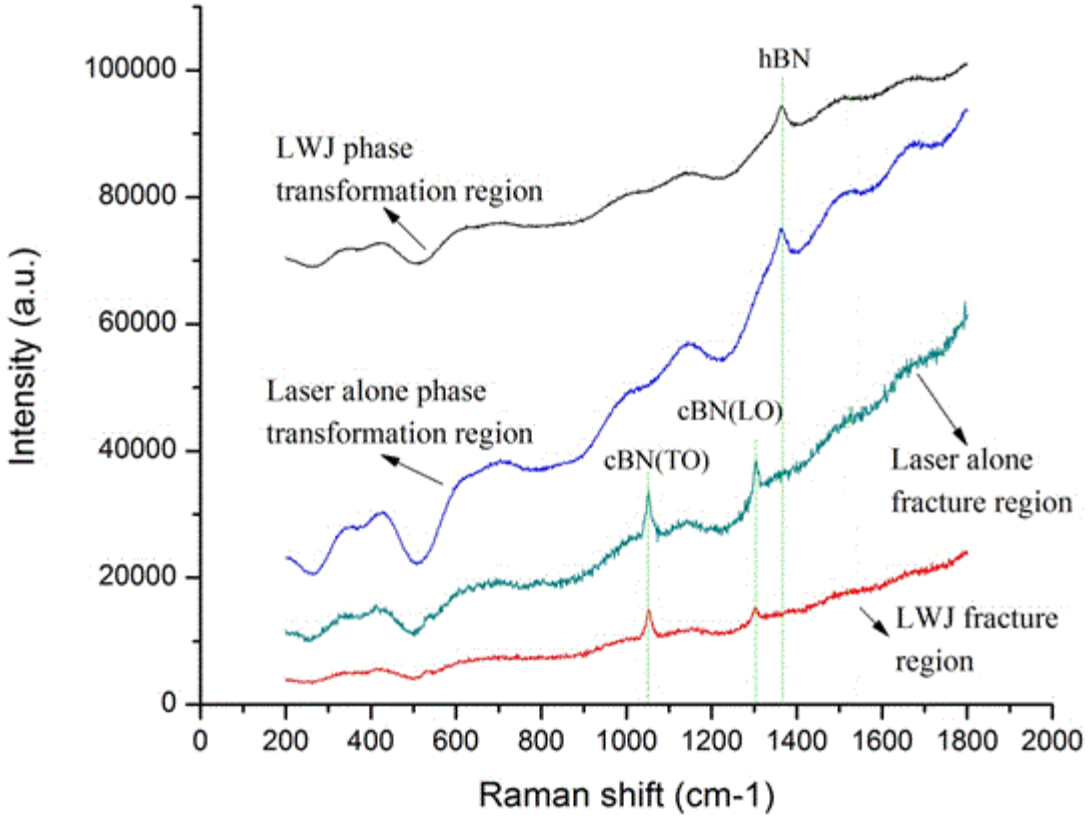

Fig. 9 Raman spectrum for transverse section of laser alone and LWJ cutting

Nitrogen was selected in the trial to cut thick PCBN due to larger depth of phase change and MMR by momentum effect. Based upon EDS and Raman spectroscopy results, our understanding of nitrogen-assisted LWJ process is divided into three stages. First is the initiation stage, where the groove was initiated by phase transformation and chemical reaction after laser irradiation. It was reported cBN undergoes phase transition to hBN at about 1800 K in the

nitrogen atmosphere[13, 14]. It is also mentioned that AlN began to oxidize at 1073 K and transformed entirely above 1273 K. Second is the groove formation stage, where hBN decomposed and the binder (AlN) reacted in air atmosphere simultaneously. As the laser passed and continuously heated up, cBN transformed into hBN and gradually decomposed into gaseous nitrogen and gaseous boron at 2400 to 2600 K[15, 16]. However the binder oxidation product (aluminum oxide) still existed at the transition zone due to the extreme high boiling point (3250 K) and inertness. Aluminum oxide acted as the main composition of the groove layer. Finally crack initiation and nucleation occurred at the transition zone, primarily due to thermal expansion mismatch stresses of BN phases and oxides. The great mismatch stresses act as the driving force to promote crack propagation and then to yield material separation.

3.4.3 FEA results

In the second set of experiments, trials at different line energies were conducted in laser alone and LWJ to predict the surface deformation and fracture characteristics by finite element analysis. Numerical modeling of surface deformation of both laser alone and LWJ process was formulated and compared to the experimental results in order to predict the transformation depth and expansion strain of the phase transformation zone. Both scribing and through cutting results were examined in laser alone and LWJ, and surface profiles are measured normal to the cutting path by an optical profilometer. The width of those grooved samples, measured by microscope was about 0.3 mm, slightly larger than the spot size of laser beam (0.2 mm). Figure 10 shows the fitting of average surface profile measurement with numerical results in both laser alone and LWJ experiment. At line energy of 94.5 kJ/m, a straight through cut was made and formed a larger deformation. In contrast, only a groove was produced at line energy of 63 kJ/m, and the

deformation induced by phase transformation was lower. The FEA results based upon numerical modeling are plotted with best fitting experimental data. In laser alone at P/v = 94.5 kJ/m, the depth of transformation used in the model is 1 mm, determined according to the measured depth of 950 μm from the SEM image. In laser alone at P/v = 63 kJ/m, predicted depth of transformation equal to 0.5 mm was found to best fit the measured surface profiles. LWJ cut through at line energy of 126 kJ/m, however only scribing was found in line energy of 94.5 kJ/m. The measured results of deformation due to phase transformation are also in good agreement with the observations. The larger slope for 126 kJ/m demonstrates more area next to cut path was transforming to hBN, however the material along the cut path were transformed entirely because overlapping part was found in both two cases. The transformation depth of through-cut used in the model is 1.2 mm, corresponding to the transverse section measurement (1100 μm) from measurement. The half width is chosen as 0.2 mm, slightly larger than the measured groove width (0.15 mm). All the solutions correspond to a constant expansion strain of 0.35%.

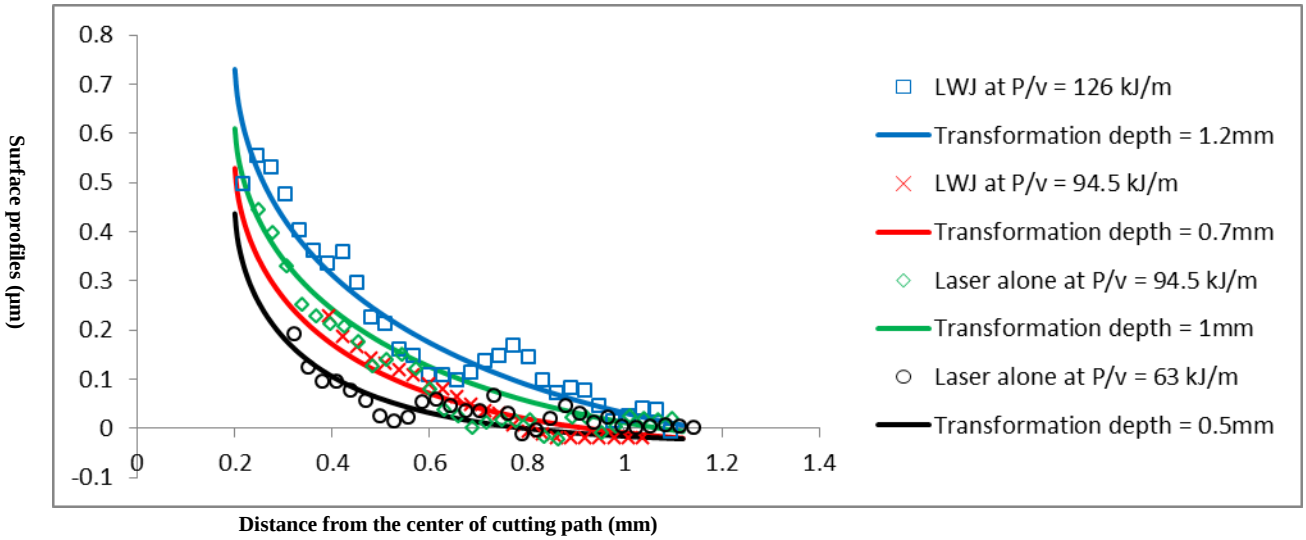

Fig. 12 Comparison of measured surface deformation and numerical prediction

The Griffith energy (G) of the plane strain crack and channeling crack were computed by the ABAQUS package (Providence, RI) and are plotted as a function of a/w (crack length to material

thickness ratio) of four series with different methods and line energies in Figure 13. Numerical calculations of energy release rates are also compared to the PCBN critical energy release rate in both cases. It has been reported that the fracture toughness (critical G) of BZN 7000S is 5-7.7 MPa$\sqrt{m}$ [17, 18]. Hence, the computed critical energy release rate ranges from 34.4 to 81.6 Pa·m. Figure 13 shows only two lines (laser alone at 94.5 kJ/m and LWJ at 126 kJ/m) exceed the critical G that possibly have the tendency to propagate the crack through, while the other two below the critical G only show scribing characteristics, which are also in agreement with the experimental results. N_2-assisted laser alone (94.5 kJ/m) and LWJ (126 kJ/m) performed through cut which also went over the critical G. In N_2-assisted laser alone (94.5 kJ/m), the energy release rate was greater than critical G for crack to 0.25 times thickness. In LWJ (126 kJ/m), the energy release rate was greater than critical G for crack to 0.35 times whole thickness. However the crack growth did not terminate, rather it extended through the whole thickness from our experimental observation. A large thermal gradient resulting in thermal shock could cause the crack initiation and separation under the critical fracture energy. Carolan et al.[19] observed that the flexural strength of PCBN with large grain size decreases rapidly accompanied by unstable crack propagation after thermal shock. This phenomenon may explain the channeling crack propagating through the cutting path under low energy release rate based upon our computation.

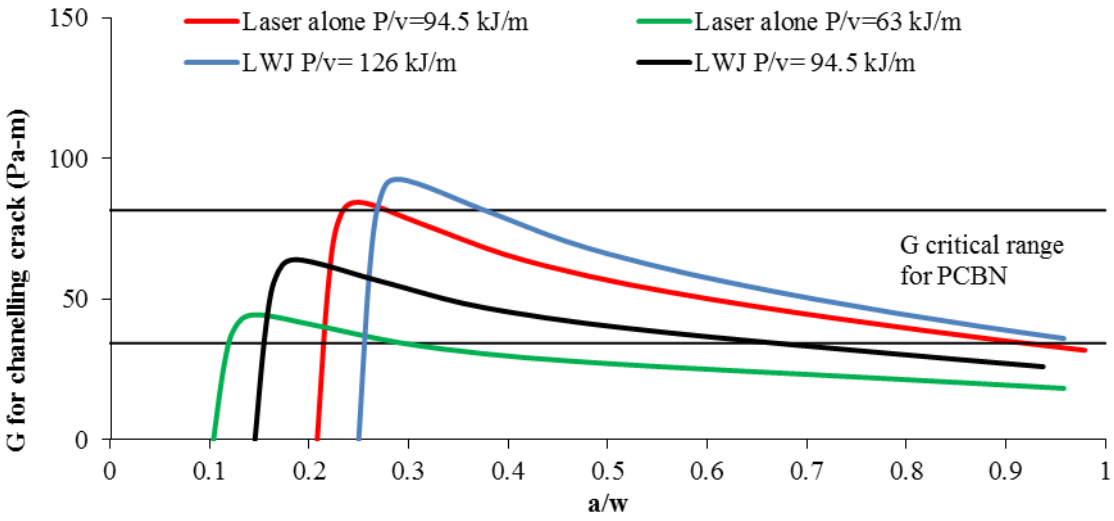

Fig. 13 Energy release rate for channeling crack

3.4.4 Process mapping of LWJ and laser alone machining

The data collected from laser alone and LWJ in both 1D and 2D cutting represented consistent results depending on cut angle and line energy (Figure 14). The critical line energy for laser alone cutting almost retained at 94.5 kJ/m from 180 ˚ to 120 ˚. However, to cut through becomes difficult at the same line energy as the cut angle decreases from 120 ˚ to 90 ˚. Given the cooling effect of waterjet, the critical line energy started to rise when LWJ cutting at the turn from 180 ˚ to 120 ˚. Only scribing was found for the 90 ˚ contour cut even at the line energy of 200.9 kJ/m. The increase of critical line energy in smaller cut angle could account for the extent of overlapping by heat affected zones in two sides which could inhibit the crack propagation at the turning point.

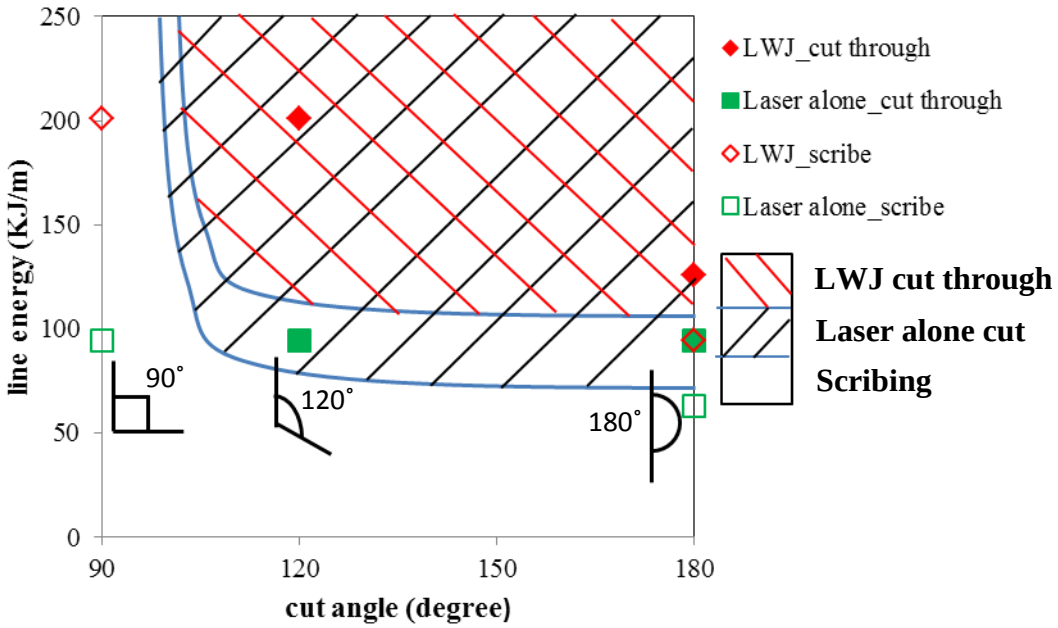

Fig. 14 Process map based upon line energy and cut angle for both laser alone and LWJ

3.5 Conclusions

Two-dimensional CO_2 laser cutting with 120 ˚ was conducted successfully at a relatively high speed (4.23 mm/s) in 4.8 mm thick solid PCBN tool blanks by means of nitrogen and waterjet. Cut quality of LWJ exhibited advantages over dry laser machining such as controlled crack trajectory at the turning point, smooth surface, small kerf width and less taper. T-stress based upon a crack path stability model was used to explain the controlled crack trajectory. Results from both EDS and Raman spectroscopy showed phase transformation such as sp^3 cBN phase to sp^2 phase like hBN and oxidation of binder material such as AlN to aluminum oxide, both leading to volumetric expansion which in turn promoted crack propagation.

Finite element analysis based computations of stress field and energy release rate were applied to help understand the mechanism of straight cut in laser alone and LWJ cutting and

predict the fracture characteristics in the experiment. Numerical modeling of surface profiles based on an expansion rate of 0.35% compared with experimental measurements was able to estimate the depth of phase transformation and region dimensions. FEA calculations of energy release rate in both plane strain and channeling crack agree well with observational results. The decrease of PCBN strength underwent severe thermal shock was introduced to explain the lower energy release rate from our calculation. FEA numerical methods can be used to predict the surface profiles as well as fracture characteristics based upon the energy release rate computation in LWJ technique.

Acknowledgements

This work is based upon the financial support by the National Science Foundation award under Grant No. CMMI-1000035. The authors also would like to express their gratitude for the polycrystalline boron nitride tool blanks donated by Diamond Innovations, Inc., Worthington, OH.

References

[1] Yogo, T., Naka, S., and Iwahara, H., 1991, "Synthesis of Cubic Boron Nitride with Boron Nitride Powder Formed from Triammoniadecaborane," Journal of materials science, 26(14), pp. 3758-3762.

[2] Pauchard A, Marco MD, Carron B et al (2008) Recent developments in the cutting of ultra hard materials using water jet-guided laser technology, ALAC conference, Minneapolis.

[3] Pauchard, A., Di Marco, M., Carron, B., Suruceanu, G., Richerzhagen, B., Brulé, A., and Kling, N., 2008, "Recent Developments in the Cutting of Ultra Hard Materials Using Water Jet-Guided Laser Technology," eds., pp.

[4] Lumely, R. M., 1969, Am. Ceram. Soc. Bull., 48(pp. 850-854.

[5] Tsai, C.-H., and Chen, H.-W., 2003, "Laser Cutting of Thick Ceramic Substrates by Controlled Fracture Technique," Journal of Materials Processing Technology, 136(1-3), pp. 166-173.

[6] Melaibari, A., Molian, P., and Shrotriya, P., 2012, "Two-Dimensional Contour Cutting of Polycrystalline Cubic Boron Nitride Using a Novel Laser/Water Jet Hybrid Process," The International Journal of Advanced Manufacturing Technology, 63(5-8), pp. 641-649.

[7] Wang, Y., Molian, P., and Shrotriya, P., 2013, "Crack Separation Mechanism in Co2 Laser Machining of Thick Polycrystalline Cubic Boron Nitride Tool Blanks," The International Journal of Advanced Manufacturing Technology, 70(5-8), pp. 1009-1022.

[8] Cotterell, B., and Rice, J. R., "On a Slightly Curved or Kinked Crack," International Journal of Fracture, 16(pp. 155-169.

[9] Yang, B., and Ravi-Chandar, K., 2001, "Crack Path Instabilities in a Quenched Glass Plate," Journal of Mechanics and Physics of Solids, 4(pp. 91-130.

[10] Kalyanasundaram, D., Molian, P., and Shrotriya, P., 2012, "Application of Chemical Transformation Induced Fracture for Cutting of Superhard Materials," Journal of Manufacturing Processes, 14(3), pp. 336-342.

[11] Ishii, T., Gonda, M., Ueda, H., Okayama, S., and Shima, N., 2001,

[12] Gurr, G., Montgomery, P., Knutson, C., and Gorres, B., 1970, "The Crystal Structure of Trigonal Diboron Trioxide," Acta Crystallograpghica Section B, 26(7), pp. 906-915.

[13] "<Properties of Diamond and Cubic Boron Nitride.Pdf>," pp.

[14] Liu, Q., Yang, G., and Zhang, J., 2003, "Phase Transition between Cubic-Bn and Hexagonal Bn Upon Pulsed Laser Induced Liquid–Solid Interfacial Reaction," Chemical physics letters, 373(1), pp. 57-61.

[15] Barin, I., Sauert, F., Schultze-Rhonhof, E., and Sheng, W. S., 1993, *Thermochemical Data of Pure Substances*, VCH Weinheim,

[16] Dreger, L. H., Dadape, V., and Margrave, J. L., 1962, "Sublimation and Decomposition Studies on Boron Nitride and Aluminum Nitride1," The Journal of Physical Chemistry, 66(8), pp. 1556-1559.

[17] D'evelyn, M. P., and Zgonc, K., 1997, "Elastic Properties of Polycrystalline Cubic Boron Nitride and Diamond by Dynamic Resonance Measurements," Diamond and Related Materials, 6(5), pp. 812-816.

[18] Tada, H., Paris, P., and Irwin, G., 1985, "The Stress Analysis of Cracks Handbook, 1973," Del Research Corporation, pp.

[19] Carolan, D., Ivanković, A., and Murphy, N., 2012, "Thermal Shock Resistance of Polycrystalline Cubic Boron Nitride," Journal of the European Ceramic Society, 32(10), pp. 2581-2586.

CHAPTER 4

CONCLUSIONS AND FUTURE WORK

4.1 Conclusions

The purpose of this work is to investigate the feasibility of using CO_2-LWJ techniques to cut thick PCBN at higher speed with better quality. Due to the non-conductivity and super hardness, cutting thick PCBN in solid form remains challenging. In this work, we studied the technique feasibility both experimentally and numerically. Continuous CO2 laser with the help of nitrogen as assist gas was able to cut through PCBN both one and two dimensionally. In addition, LWJ was found to cut through in higher line energy but better cut quality.

One dimensional CO_2 laser cutting experiments were conducted on 4.8 mm thick solid PCBN tool blanks with the assistance of nitrogen and waterjet. The 2^3 factorial design of experiments (DOE) was applied to determine the main effects and interaction effects of laser power, cutting speed, and gas/waterjet pressure on phase transformation depth, R_a, and taper angle. Results showed material removal occurred beginning with the phase transformation of cBN to hBN, followed by the decomposition of hBN and chemical reactions with water, and ending with crack separation. Waterjet improved the cut quality by a smaller phase transformation depth, less taper, and finer fracture zone compared to nitrogen although the latter required less line energy for cutting. The statistical analysis revealed laser power followed by waterjet pressure had the most significant effects among all the factors.

Two-dimensional CO_2 laser cutting with 120˚ was conducted successfully at a relatively high speed (4.23 mm/s) in 4.8 mm thick solid PCBN tool blanks with the combination of nitrogen and waterjet. Cut quality of LWJ exhibited advantages over dry laser machining such as controlled crack trajectory at the turning point, smooth surface, small kerf width and less taper.

Results from both EDS and Raman spectroscopy shown phase transformation including sp^3 cBN phase to sp^2 phase like hBN and oxidation of binder material such as AlN to aluminum oxide, both leading to volumetric expansion caused crack initiation and propagation.

Finite element analysis based computations of stress field and energy release rate were applied to help understand the mechanism of straight cut in laser alone and LWJ cutting and predict the fracture characteristics in the experiment. Numerical modeling of surface profiles based on expansion rate of 0.35% compared with experimental measurements was able to estimate depth of phase transformation and region dimensions. FEA calculations of energy release rate in both plane strain and channeling crack agree well with observational results. The decrease of PCBN strength underwent severe thermal shock was introduced to explain the lower energy release rate from our calculation. FEA numerical methods could provide an essential guide for predicting the surface profiles as well as fracture characteristics based upon the energy release rate computation in LWJ technique.

4.2 Future works

N_2-assisted LWJ cutting thick PCBN in acute angle

One of the limitations of this work is merely cutting acute angle contour. There is still further exploration to overcome the bottle neck, both in technique and in mechanism. The solution we will perform includes separating 2D machining into two 1D cut separately.

Study the effects of variables in two dimensional cutting

The statistical study of both main and interaction effects was helpful to predict and design the experiment. There are also several factors of interest to be determined in the 2D machining

experiments. For example, laser power, cutting speed, cut angle, fluid media and waterjet pressure could affect the cut quality and fracture characteristics. The study will help us figure out the experimental parameters and understand the mechanism of 2D cutting.

CO_2-LWJ cutting thick PCD material

Diamond is the hardest material as known, superior to cBN. It is meaningful to investigate the feasibility of applying hybrid CO_2-LWJ in cutting thick PCD blank. The higher hardness and thermal conductivity remains to be a challenge in our future work.